Structural asymmetry in biotic interactions as a tool to understand and forecast ecological persistence

Alfonso Allen-Perkins[1,*], David García-Callejas[2,3], Ignasi Bartomeus[4], and Oscar Godoy[5]

[1]Departamento de Ingeniería Eléctrica, Electrónica, Automática y Física Aplicada, ETSIDI, Technical University of Madrid, 28040 Madrid, Spain.

[2]School of Biological Sciences, University of Canterbury, Private Bag 4800, Christchurch 8140 New Zealand.

[3]Landcare Research, Lincoln, New Zealand.

[4]Estación Biológica de Doñana (EBD-CSIC), Seville, Spain.

[5]Instituto Universitario de Ciencias del Mar (INMAR), Departamento de Biología, Universidad de Cádiz, E-11510, Puerto Real, Spain.

[*]Correspondence: alfonso.allen.perkins@gmail.com

Abstract

A universal feature of ecological systems is that species do not interact with others with the same sign and strength. Yet, the consequences of this asymmetry in biotic interactions for the persistence (i.e. long-term viability) of individual species and entire communities remains unclear. To address this gap of knowledge, we conceptualize in this perspective these ecological observations by implementing a set of tools into the field of structural stability. By quantifying independently the size from the shape of the so-called feasibility domain, we show that it is possible to obtain simultaneously an understanding of the opportunities for all species within a community to persist as well as the vulnerability of individual species to extinction under changing environmental conditions. We further demonstrate that these novel metrics carry also predictive value. Specifically, the shape-related metrics predict annual changes in species abundances during seven years in a Mediterranean grassland. Our approach, which is designed to be applied to any ecological system regardless of their number of species and type of interactions, shows that is possible to obtain both mechanistic and predictive information of ecological persistence across levels of organization, providing a clear link for a stronger integration of theoretical and empirical research.

Introduction

Ecologists seek to obtain a mechanistic understanding of the processes governing the dynamics of ecological systems. The meaning of *mechanistic*, however, varies across ecological levels of organization. For instance, while biotic interactions are key for a mechanistic understanding of species dynamics in community ecology (Levine *et al.*, 2017), so is plant growth for population ecologists or photosynthesis rates for ecophysiologists (Peñuelas *et al.*, 2011). Nevertheless, a common trade-off across fields is that obtaining such mechanistic understanding often comes at the cost of losing predictive ability (Dietze, 2017; Petchey *et al.*, 2015b; Tredennick *et al.*, 2021). These mismatches between understanding ecological processes and predicting ecological dynamics are due to multiple causes, yet a common limitation is the lack of correspondence between the mathematical tools used for understanding and those used for predicting. For instance, in community ecology, while the mechanistic understanding of complex dynamics of interacting species uses well-established population models (Bimler *et al.*, 2018; Godoy & Levine, 2014), predictive studies are much less developed, and generally use a completely different set of tools including black-box approaches such as machine learning and neural networks (Civantos-Gómez *et al.*, 2021; Evans *et al.*, 2011).

In order to break the methodological trade-off between understanding and forecasting, recent approaches have applied tools from the structuralist approach (Saavedra *et al.*, 2020; Song *et al.*, 2020). In mathematics, structural stability is a fundamental property of dynamical systems which defines the range of conditions compatible with stable dynamics. The structuralist view in ecology has been used to provide a set of simple explanations to understand the diversity (or lack thereof) we observe in nature (García-Callejas *et al.*, 2021; Saavedra *et al.*, 2017). The central mechanism is that the structure of species interactions influences the opportunities for multiple species to persist in the long term and, therefore, their coexistence (Godoy *et al.*, 2018). The larger these opportunities are (measured as the size of the so-called feasibility domain), the larger the range of environmental conditions the community can withstand without losing any species. Among other insights, it has been predicted (Saavedra *et al.*, 2017), and empirically shown (Bartomeus *et al.*, 2021) that this situation occurs when species experience strong self-regulation and niche differentiation. These insights are probabilistic in nature (Cenci *et al.*, 2018), coherent with the

principle that is impossible to quantify the whole set of abiotic and biotic factors modulating community dynamics (Shoemaker *et al.*, 2019).

The occurrence, sign, and strength of biotic interactions are arguably the most relevant information needed to understand and predict ecological outcomes at both the species and the community level (MacArthur, 1957). As such, biotic interactions are the raw material that the structuralist approach uses to define the size of the feasibility domain, which in turn allows predicting the persistence of whole communities (i.e., community feasibility), species composition, or abundances at equilibrium (Tabi *et al.*, 2020). For instance, it has been shown that in both random and empirical communities, the size of the feasibility domain (i.e. the range of species growth rate values compatible with persistent communities) is dependent on the type of interaction, mean interaction strength, and connectance (Grilli *et al.*, 2017). However, whether species interactions on average are strong or weak as well as their distribution is not only relevant to determine the size, but equally important as well, the shape of the feasibility domain. Conceptually speaking, if all species interact in the same way the feasibility domain will be symmetrical, but in practice a common feature of real world systems is that interactions among species are asymmetric (Adler *et al.*, 2018; Bascompte *et al.*, 2006). This asymmetries in interactions translates to asymmetries in the feasibility domain as exemplified in a recent work on empirical mutualistic networks (Grilli *et al.*, 2017).

Understanding the asymmetry of the feasibility domain is important because it implies that not all species have the same opportunities to coexist. That is, some species are more affected than others by changes in environmental conditions. Therefore, even in communities with large feasibility domains, it is likely that particular species may become locally extinct when environmental conditions change. These more vulnerable species represent the "weak spot" for the feasibility of the whole community (Grilli *et al.*, 2017). This process was exemplified in a recent study by Tabi *et al.* (2020) who, working with protist communities in temperature-controlled environments, showed that in communities with more asymmetric feasibility domains, there is a lower capacity to predict the identity of which protists went extinct first. Overall, these examples are showing that it is not only important to understand the potential of the community structure to maintain

all of its constituent species, but also the relative vulnerability of each species to perturbations in their demographic performance.

Despite these recent studies providing solid and rigorous progress, it is still poorly understood how to independently quantify the shape and the size of the feasibility domain. Performing this separation is critical to better predict ecological outcomes at different levels of ecological organization (species versus community). Conceptually, we should aim for a shape measure that is independent of the size of the feasibility domain. Although these properties are not fully independent (see an example in Suppl. Section 1), it is currently not explored to what extent they can be meaningfully disentangled and interpreted. For instance, when measuring the shape of the feasibility domain as the heterogeneity in the distribution of the side lengths of the borders (Grilli *et al.*, 2017), we are implicitly measuring the change in the size of the domain as well. This is because a mild increase in the variability of the side lengths of the feasibility domain implies also an increase in its size. A similar conceptual problem applies to characterizing the asymmetry of the feasibility domain by computing the variability of the direct effect of one species over the rest (Tabi *et al.*, 2020). To advance in our ability to predict the dynamics of ecological communities, we provide in this perspective new developments that control for the correlation between the shape and size of the feasibility domain. Failing to control for this size-shape relationship may significantly hinder our ability to estimate species' vulnerabilities to exclusion in local communities.

Coupled with these advances in theory and associated tools, we require empirical tests to evaluate their usefulness. Otherwise, they will remain valid theoretical constructs but with little application to real conditions. Predictions of ecological dynamics using the structuralist approach have focused so far on either computer simulations (Grilli *et al.*, 2017) or highly controlled laboratory (Tabi *et al.*, 2020) and experimental settings (Bartomeus *et al.*, 2021), yet we lack hard tests under field conditions. These tests are key to shed light on the applicability of the perspective we present here to forecast species dynamics across a wide range of ecological systems and environmental conditions. The litmus test of ecological prediction is that of forecasting species abundances (Clark *et al.*, 2020; Tredennick *et al.*, 2017), which is relatively uncommon due to its inherent complexity, as it encompasses a greater degree of information than species richness or

composition (McGill *et al.*, 2007).

In this perspective, we develop and test new probabilistic metrics to understand species' relative vulnerability to exclusion from local communities, and the relationship of these metrics with observed abundances in complex communities. In particular, we first present an extension of the geometrical approach of structural stability to robustly quantify 1) the minimum perturbation that can exclude a given species from a feasible community (denoted here as "exclusion distance"), 2) the absolute and relative probabilities of being the first species excluded from the community (referred as "average probability of exclusion" and "exclusion ratio", respectively), and 3) an intuitive index that quantifies the asymmetry in species' vulnerabilities to extinction in any ecological community, regardless of their overall feasibility potential (referred as the "feasibility asymmetry index"). Importantly, these metrics can be applied to ecological communities with arbitrary interaction types and number of species. Second, we ask whether these metrics can inform about the expected abundance of species through time in a diverse grassland community. We show that the metrics developed here, i.e. the probability of exclusion of species in a given year, are phenomenologically correlated with species abundances in the following year.

Theoretical framework

Preliminaries: Definition of the feasibility domain and its size

To help the reader understand the theoretical background of this perspective, we briefly introduce some key concepts of the structuralist approach. This theoretical framework posits that the structure of species interactions determines the opportunities for species to coexist by conditioning the size of the feasibility domain. Particular structures of species interactions, such as intraspecific competition exceeding interspecific competition, promote larger sizes of the feasibility domains and, therefore, larger opportunities for species to coexist (Saavedra *et al.*, 2017) (see García-Callejas *et al.* (2023) for a recent empirical example). In order to measure the size of the feasibility domain, we need to connect the structure of species interactions with a model that describes reasonable well the dynamics of interacting species. The underlying model commonly used is the linear Lotka-

Volterra (LV) model, as it represents a balance between tractability and complexity, and it is the linearized, general version of other population models with more complex formulations (Cenci & Saavedra, 2018; Hart *et al.*, 2018; Saavedra *et al.*, 2017). On the one hand, the model allows summarizing the effect of the abiotic and biotic environment on the performance (i.e., the balance between mortality and resource intake) of individual species into a single parameter, the intrinsic growth rate (Saavedra *et al.*, 2020). On the other hand, despite its simplicity, the LV model has successfully explained and predicted the dynamics of diverse ecological systems under controlled and natural experimental conditions (García-Callejas *et al.*, 2021; Godoy & Levine, 2014; Saavedra *et al.*, 2020; Tabi *et al.*, 2020; Venturelli *et al.*, 2018). The model is of the form:

$$\frac{\mathrm{d}N_i}{\mathrm{d}t} = N_i \left(r_i + \sum_{j=1}^{S} \alpha_{ij} N_j \right), \tag{1}$$

where the variable N_i denotes the abundance of species i, S is the number of species, the parameter r_i is the intrinsic growth rate of species i which represents how species i grows in isolation under given abiotic conditions, and α_{ij} is the element (i, j) of the interaction matrix $\mathbf{A}$ and represents the per-capita biotic effect of species j on the per-capita growth rate of species i.

For a given ecological community, the necessary conditions that sustain positive abundances for all its constituent species across time depends on its interaction matrix $\mathbf{A}$, and are known as the feasibility domain of the community, denoted by $D_F(\mathbf{A})$. Formally, $D_F(\mathbf{A})$ is the parameter space of intrinsic growth rates that leads to a feasible (positive) equilibrium, i.e., the set of $\mathbf{r}$ such that $\mathbf{N}^* = -\mathbf{A}^{-1}\mathbf{r} > \mathbf{0}$ for non-singular interaction matrices $\mathbf{A}$ (i.e., for matrices whose inverse, denoted as $\mathbf{A}^{-1}$, exists), where $\mathbf{r}$ is a column vector whose i-th element is the intrinsic growth rate r_i, and $\mathbf{N}^*$ is a column vector whose i-th element represents the abundance of species i when the feasible equilibrium exists, $N_i^* > 0$ (Song *et al.*, 2018). When the points in $D_F(\mathbf{A})$ are also stable (i.e., when the real part of the eigenvalues of the linearized Jacobian matrix of Eq. (1) is negative), then feasibility ensures the stable coexistence of the S species (Logofet, 2005). However, since stability is usually difficult to prove (Logofet, 2005), especially when studying empirical communities, hereafter we restrict our analyses to feasibility, the necessary condition for species coexistence understood as long-term viability.

According to the structuralist approach, the larger the size of the feasibility domain, the more likely the community can persist without any species going extinct. To quantify its size, previous work has assumed that we do not have any a priori knowledge about how the intrinsic growth rates will change within a community. For that reason, we assume that all parameter values are equally likely to be observed in the entire parameter space (Saavedra *et al.*, 2020), and use the probability of uniformly sampling a vector of feasible intrinsic growth rates on a representation of that space, the unit-ball. The unit-ball of a community with S species, B^S, is defined as the set of all vectors of intrinsic growth rates $\mathbf{r}$ that satisfy

$$r_1^2 + r_2^2 + \cdots + r_S^2 = 1 \text{ for } \mathbf{r} = \begin{pmatrix} r_1 \\ r_2 \\ \vdots \\ r_S \end{pmatrix}. \tag{2}$$

In mathematical terms, the probability that all species can persist is equal to the normalized solid angle $\Omega(\mathbf{A})$, defined by the ratio of the following volumes:

$$\Omega(\mathbf{A}) = \frac{\text{vol}\left(D_F\left(\mathbf{A}\right) \cap B^S\right)}{\text{vol}\left(B^S\right)}, \tag{3}$$

where $X \cap Y$ denotes the intersection of any two sets X and Y (Gourion & Seeger, 2010; Saavedra *et al.*, 2020, 2015; Song *et al.*, 2018). To illustrate these mathematical expressions for a community with three species, Fig. 1 shows the intersection of the feasibility domain with the unit-ball. Specifically, only the points that lie within those triangles represent feasible vectors of growth rates. The vertices in Fig. 1 (colored circles) depict vectors of intrinsic growth rates where only a single species has positive equilibrium abundances $N_i^* > 0$ ($N_j^* = 0$ for $i \neq j$), whereas each edge shows vectors of growth rates where a given species (the species of the vertex with the same color as the edge) goes excluded. Importantly, both communities in Fig. 1 have feasibility domains with the same relative volume Ω ($\Omega = 0.064 =$ area of the spherical triangle/area of the unit-ball) but differ in their shape. For communities with S species, the relative volume $\Omega(\mathbf{A})$ is a non-negative quantity that lies between 0 and 0.5 (Song *et al.*, 2018). That means that the closer $\Omega(\mathbf{A})$ is to 0.5,

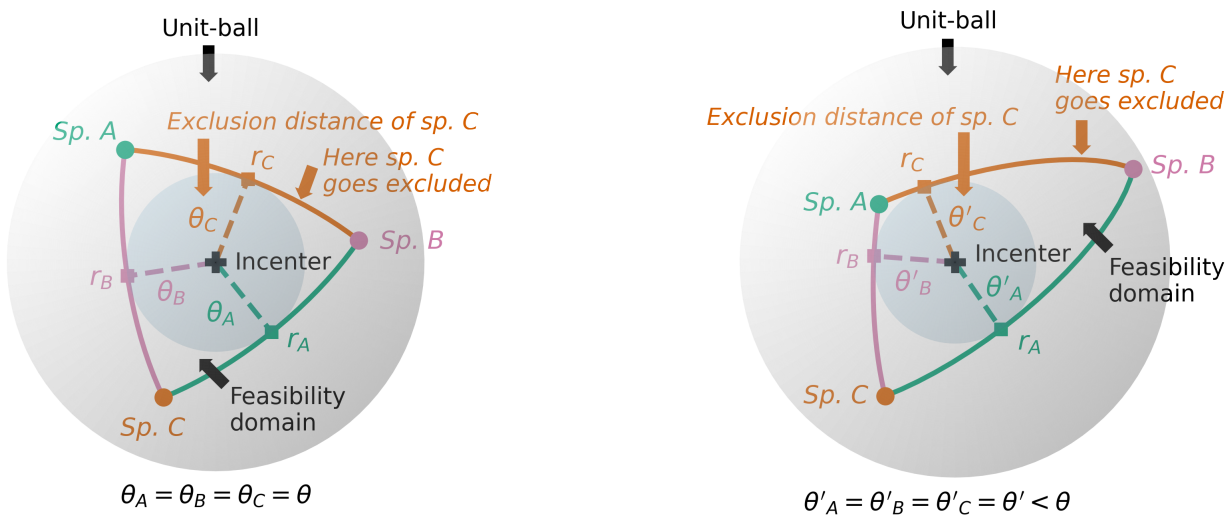

(a) (b)

Fig. 1: Examples of feasibility domains for communities with $S = 3$ species. The white sphere represents the unit-ball, whereas the spherical triangles show the borders of the feasibility domain. Within the spherical triangles lie the vectors of intrinsic growth rates that lead to the persistence of the three species altogether. In this example, the relative volume of both triangles (Ω) is the same. However, in panel (a) we represent a symmetric domain (equilateral spherical triangle), whereas panel (b) shows an asymmetric one (scalene spherical triangle). The distance between the incenters of the feasibility domain(black plus markers) and their respective borders (square markers) are represented with dashed colored lines, and, in addition, the blue spherical caps are a guide to the eye to compare that the minimum distance from the incenter to the edge of the feasibility domain is shorter in the asymmetric triangle. This asymmetry due to variation in species interaction makes species C (represented by orange color) more susceptible to be excluded than species A (represented by green color).

the larger the likelihood that the structure of species interactions $\mathbf{A}$ promotes a feasible community regardless of the differences in intrinsic growth rates among species. The relative volume $\Omega(\mathbf{A})$ presented in Eq. (3) can be efficiently calculated by computing the following expression:

$$\Omega(\mathbf{A}) = \frac{1}{(2\pi)^{S/2}\sqrt{|\det(\mathbf{A})|}} \int \cdots \int_{\mathbf{N}^* \geq 0} e^{-\frac{1}{2}\mathbf{N}^{*T}\mathbf{A}^T\mathbf{A}\mathbf{N}^*} \mathrm{d}\mathbf{N}^*, \tag{4}$$

via a quasi-Monte Carlo method (Genz & Bretz, 2009; Genz *et al.*, 2021; Saavedra *et al.*, 2016a; Song *et al.*, 2018).

Feasibility domain' shape: Interpreting perturbations as distances

The size of the feasibility domain (which is proportional to its relative volume Ω) can be used as an indicator of the tolerance of a community to random environmental variations. However, two communities with the same number of species S and identical values of Ω can still have very different responses to perturbations of their intrinsic growth rates $\mathbf{r}$, depending on the shape of their feasibility domains (see Fig. 1). Because this shape is therefore critical to better understand and predict the feasibility of the whole community and the vulnerability of its constituent species, we here present and develop four metrics to thoroughly characterize such shape, namely: 1) the species exclusion distances, 2) their average probabilities of exclusion, 3) their exclusion ratios and, at the community level, 4) the feasibility asymmetry index (see Box 1 for a brief summary of those metrics).

Box 1 — Metrics based on the feasibility domain' shape.

Species exclusion distance. Given a feasible community whose dynamics can be reasonably well approximated with a linear LV or equivalent models (see Eq. (1) and Saavedra *et al.* (2017)), the exclusion distance of species i, denoted as θ_i, represents the minimum perturbation of the community's initial vector of intrinsic growth rates ($\mathbf{r}_0$) that can exclude species i from that community. The geometrical definitions and reasoning required for its analytical calculation (see Eq. (S7)) are presented in Suppl. Sections 2 and 3.

Average probability of exclusion. This probabilistic metric, denoted as P_i^E, ranges between 0 and 1, and estimates the average (absolute) probability that species i will be the first one to be excluded if a destabilizing perturbation took place in a feasible community under LV dynamics. According to its formal definition (see Eqs. (5) and (8)), on the one hand, the calculation of these probabilities does not require an initial vector of intrinsic growth rates. On the other hand, their values mainly depend on the shape of the feasibility domain. In ideal symmetric communities with S species, all species are equally likely to be the first species excluded and, consequently, the average probability of exclusion of each species is given by $P_i^E = 1/S$.

Species exclusion ratio. Given a community with S species, the exclusion ratio of species i, denoted as ER_i, is a relative metric that assesses whether the average probability of exclusion for species i (P_i^E) is large by comparing it to that of an ideal symmetric community with the same number of species ($1/S$) (García-Callejas *et al.*, 2023) (see Eq. (6)). By definition, this metric ranges between 0 and infinity, and is equal 1 only in symmetric communities. The larger the exclusion ratio of species i, the larger the relative probability that i can be the first species that goes excluded.

Feasibility asymmetry index. This community-level metric describes the distribution of the average probabilities of exclusion $P_i^E(\mathbf{A}) \in [0, 1]$ and, thus, the (a)symmetry of the feasibility domain' shape. To quantify it, we use a commonly-used equitability index (sensu Tuomisto (2012)): the relative Shannon diversity index of the average probabilities of exclusion $P_i^E(\mathbf{A})$ (see Eq. (9)).

To introduce these metrics, we start by answering a simple question: What is the maximum perturbation in environmental conditions a community can withstand without losing species and therefore becoming unfeasible? To answer this question, first, we should consider that species go excluded when the vector of growth rates of the community $\mathbf{r}$ moves from its initial position until it reaches the border of the feasibility domain, due to the perturbation. The further away a vector of intrinsic growth rates $\mathbf{r}$ is from the border of the feasibility domain, the larger the perturbations of $\mathbf{r}$ the community can withstand while being feasible. The largest minimum distance between a vector of growth rates $\mathbf{r}$ and the border occurs when the vector $\mathbf{r}$ is at the *incenter* of the feasibility domain $\mathfrak{I}$ (see black plus markers in Fig. 1) because its minimum distance to any edge of the feasibility domain is the same regardless of the direction of the perturbation (i.e isotropic perturbation). Thus, the maximum isotropic perturbation that a community can cope with, while being feasible, will be geometrically equivalent to the distance from the incenter to all the edges of the feasibility domain (along the surface of the unit-ball), denoted by θ (see dashed lines in Fig. 1).

Now we can ask how the shape of the feasibility domain influences the maximum perturbation of the incenter $\mathfrak{I}$. In general, when two communities follow Eq. 1 and have the same number of species S and equal sizes of their feasibility domains, the more asymmetric a feasibility domain

is, the closer the edges are to the incenter $\mathfrak{I}$ and, consequently, the smaller the minimum distance between them θ (i.e., the smaller maximum perturbation). This difference is illustrated in our example for $S = 3$ species in Fig. 1, where the maximum isotropic perturbation from the incenter is larger for the symmetric domain than for the asymmetric one ($\theta_{\text{symmetric}} = 0.417$ and $\theta_{\text{asymmetric}} = 0.365$, respectively). The calculations required to find the incenter $\mathfrak{I}$ and the maximum isotropic perturbation θ of a given interaction matrix $\mathbf{A}$ can be found in Suppl. Section 2. Nevertheless, this example is a simplistic approximation. The more likely case we can find in nature is that communities that differ in the size of the feasibility domain because they have a different structure of species interactions, or that they even differ in their species richness. This variation in the size and number of species will consequently affect the shape of the feasibility domain. The next sections are therefore dedicated to explain under realistic conditions how changes in the shape of the feasibility domain allow us to understand and predict the magnitude of perturbations that species can withstand (exclusion distance) and the average probability of exclusion for species and entire communities.

Feasibility domain' shape: Species exclusion distances

In the previous section, to answer the question of which is the maximum (isotropic) perturbation a community can handle without losing species, we considered the distance from a specific point, the incenter ($\mathfrak{I}$), to the edges of the feasibility domain (θ). However, the same question can be explored by taking any other initial vector of intrinsic growth rates within the feasibility domain $\mathbf{r}_0 \neq \mathfrak{I}$. In this more general case, we can find the point in the border of the feasible domain ($\mathbf{r}_{0,\text{min}}$) at a minimum distance (along the surface of the unit-ball) to the initial vector of growth rates ($\mathbf{r}_0$). That distance between $\mathbf{r}_0$ and the closest point in the border $\mathbf{r}_{0,\text{min}}$, θ_0, defines the maximum perturbation that will cause one of the S species to be excluded. The advantage here is that the approach can further inform us about which species will go extinct first: The identity of such species only depends on the location of $\mathbf{r}_{0,\text{min}}$ on the border of the feasibility domain. Following the example in Fig. 2(a), the closest point to the initial vector of growth rates $\mathbf{r}_0$ (blue circle) that is located in the border of the feasibility domain is $\mathbf{r}_C \equiv \mathbf{r}_{0,\text{min}}$ (orange square), and it is located

in the edge where species C is excluded (orange edge).

In many situations, e.g. in conservation and restoration efforts, we are interested in the persistence of particular species, which poses the question of whether we can calculate such maximum perturbation before losing a given species i from the community. To do so, we simply need to calculate the minimum distance (along the unit-ball) from $\mathbf{r}_0$ to the edge of the feasibility domain where i goes excluded, denoted by $\theta_{0,i}$. This distance is what we define as *species exclusion distances*. In Fig. 2(a), we represent the exclusion distances for the initial vector of growth rates $\mathbf{r}_0$ with dashed lines.

Feasibility domain' shape: Average probabilities of exclusion and exclusion ratios

In order to estimate the species exclusion distances θ_i we need quite a lot of information on the system, namely: the structure (matrix) of species interaction $\mathbf{A}$, which defines the feasibility domain $D_F(\mathbf{A})$, along with a vector of intrinsic growth rates, $\mathbf{r}_0$. However, characterizing such vector can be a challenging, labor-intensive work even in small communities (Bartomeus *et al.*, 2021), and, hence, this information is not available for many communities, usually those including animal and long-lived species. In these cases, we can use the above definitions and a probabilistic perspective to estimate $P_i^E(\mathbf{A})$, the average probability that species i will be the first one to be excluded if a strong perturbation took place:

$$P_i^E(\mathbf{A}) = \frac{\mathrm{vol}\left(r_0 \in \left(D_F\left(\mathbf{A}\right) \cap B^S\right) \mid \mathbf{r}_{0,\min} \in \varepsilon_i\right)}{\mathrm{vol}\left(D_F\left(\mathbf{A}\right) \cap B^S\right)}, \tag{5}$$

where ε_i represents the edge of the feasibility domain in which species i goes excluded. Note that this probability is formulated independently from the precise specification of initial conditions, similarly to the structural forecasting in Saavedra *et al.* (2020). According to Eq. (5), the probability $P_i^E(\mathbf{A})$ corresponds to the proportion of the feasibility domain's volume (within the unit-ball) where the vectors of intrinsic growth rates are closer to the edge where species i is excluded (see Fig. 2). Therefore, by definition, $P_i^E(\mathbf{A}) < 1$ for $S > 1$ (when $\mathbf{A}$ is non-degenerate). We name the

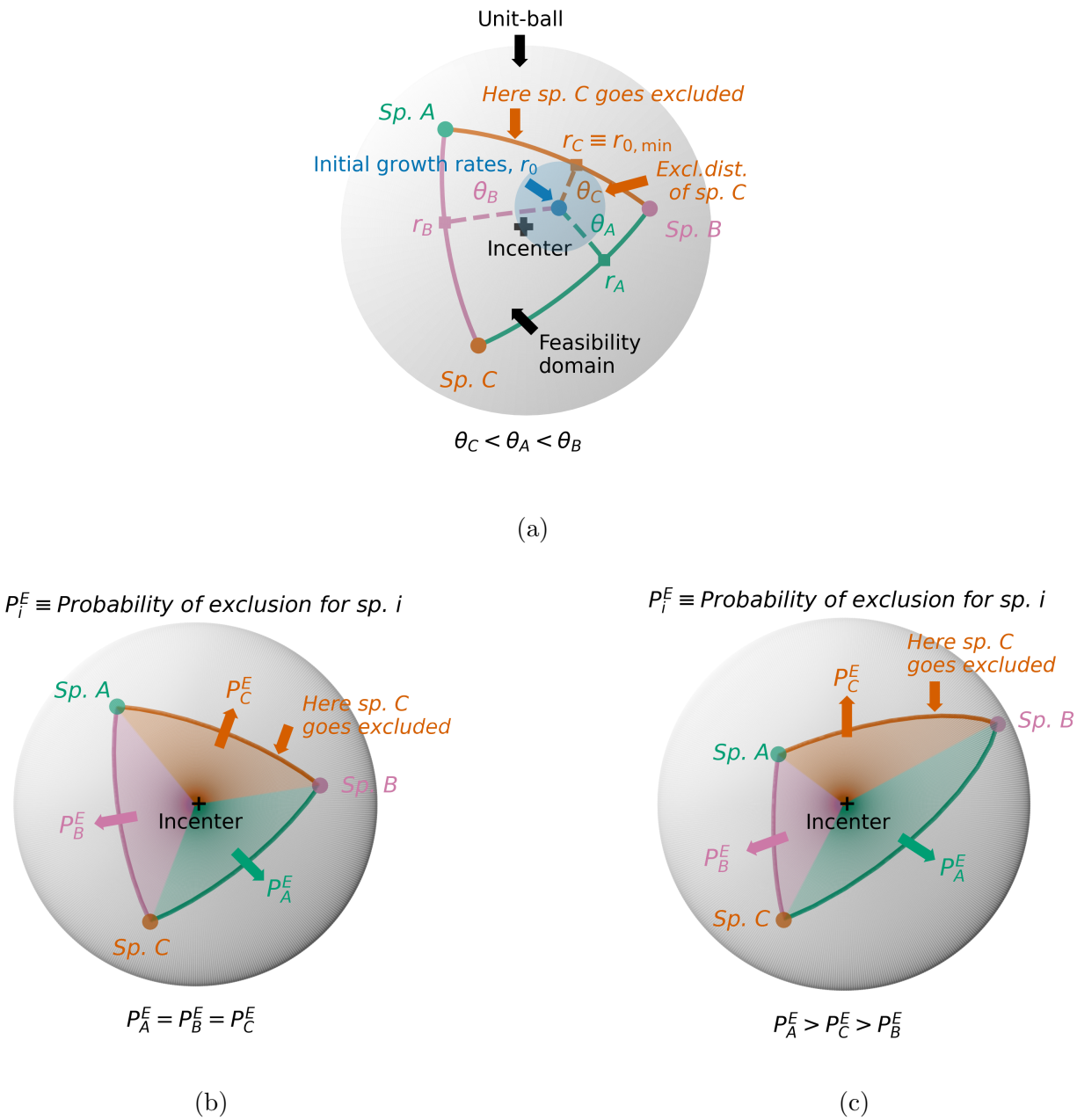

Fig. 2: (a) Exclusion distances θ_i and maximum perturbation $\theta_0 (\equiv \theta_C)$ for the community in Fig. 1(a) when the initial vector of growth rates $\mathbf{r}_0$ (dark blue dot) is not at the incenter (black plus marker). Dashed lines represent the exclusion distances (i.e., the shortest distances along the unit-ball from the initial vector of growth rates (r_0) to the border where a given species goes extinct (square markers)). The colors of squares and dashed lines are those of the species excluded. (b) Representation of the average probabilities of exclusion for the species in the feasibility domain shown in Fig. 1(a). The colors correspond to those of the species that will be the first ones to be excluded. (c) This panel shows the same information in Fig. 2(b) for the feasibility domain in Fig. 1(b).

quantity $P_i^E(\mathbf{A})$ as the *average probability of exclusion for species i*.

The average probability of exclusion of a given species depends on the size and shape of the feasibility domain. As Fig. 2 illustrates, such probabilities are mainly conditioned by the distance between the species vertices (circles) and the incenter (plus markers): the closer the vertex of a given species is to the incenter $\mathfrak{I}$ (compared to other vertices), the larger the probability that such species will be the first one to be excluded, and therefore the whole community will not be longer feasible. This last prediction is important because it implicitly indicates that the shape of the feasibility domain can be characterized by computing the average probabilities of exclusion. For instance, in communities where all species interact in the same way, and consequently have symmetric feasibility domains, all vertices are at the same distance from the incenter, and the average probability of exclusion is the same for all species $P_i^E(\mathbf{A}) = 1/S$ (see Fig. 2(b) for an example). In contrast, the larger the variation across the probabilities of exclusion, the larger the asymmetry of the feasibility domain because species present also asymmetries in their interaction matrix (e.g. effect on species i on j is not the same as the effect on species j on i). Our approach allow to assess whether the average probability of exclusion for a given species is large by comparing it to a situation in which all species interact in the same way and therefore are equally likely to be the first species excluded:

$$ER_i(\mathbf{A}) = \frac{P_i^E(\mathbf{A})}{1/S}. \tag{6}$$

We denote such quantity as the *species exclusion ratio* (García-Callejas *et al.*, 2023). If $ER_i(\mathbf{A}) < 1$ ($ER_i(\mathbf{A}) > 1$), then the probability of exclusion of species i is smaller (larger) than that of a symmetric community. So we hypothesize that the smaller the value of $ER_i(\mathbf{A})$, the larger the species probability of persistence. Note that Eq. (6) can be generalized by replacing the term $1/S$ (i.e., the symmetric probability of exclusion) by an average probability of exclusion derived from a null model approach:

$$ER_i(\mathbf{A}) = \frac{P_i^E(\mathbf{A})}{P_i^E(\mathbf{A}^{\text{Null}})}, \tag{7}$$

where $\mathbf{A}^{\text{Null}}$ represents a random interaction matrix constructed by applying a null model to matrix $\mathbf{A}$.

Finally, to compute the average probabilities of exclusion $P_i^E(\mathbf{A})$ in Eq. (5) and the exclusion ratios derived from them in Eqs. (6) and (7), we propose the following approach:

$$P_i^E(\mathbf{A}) = \frac{\Omega\left(\mathbf{A}_i^M\right)}{\Omega\left(\mathbf{A}\right)}, \tag{8}$$

where $\mathbf{A}_i^M$ represents a modified interaction matrix, obtained by replacing the vertex of species i (V_i) by the incenter, $\mathfrak{I}$, which is equivalent to replace the $i-$th column of $\mathbf{A}$ by the negative of the incenter's column vector. Intuitively, the solid angle $\Omega\left(\mathbf{A}_i^M\right)$ is the proportion of the volume of the unit-ball where the vectors of growth rates are closer to the edge where species i is excluded (i.e., $\mathbf{r}_{0,\min} \in \varepsilon_i$. If we consider the examples in Figs. 2(b) and (c), we simply say that the area occupied by a given color (e.g. green) is equal to the area obtained when placing the green vertex of species A in the position of the incenter.

It is worth noting that by using the same quasi-Monte Carlo method applied to estimate Eq. (4), we can compute efficiently both the numerator and denominator in Eq. (8), and the results obtained are in excellent agreement with those obtained by simulating the dynamics of the underlying LV model (Eq. 1) (see Suppl. Section 4 for details on the LV simulations, as well as examples in communities with three and more species). This might seem a technical detail but it has important implications for the application of our metrics by a broad range of ecologists. The problem we solve here is that finding several initial conditions randomly for estimating $P_i^E(\mathbf{A})$ from numerical simulations is a time-intensive task when the relative volume of the feasibility domain is small ($\Omega \lesssim 10^{-12}$) with orders of magnitude that vary from minutes-hours with our approach to days-weeks with the numerical LV estimation (see Fig. S5 for an example). On top of this problem, solving the LV model numerically can be far from trivial when the abundance of certain species grows indefinitely, as in communities with mutualistic interactions and weak self-regulation. For those reasons, the estimation of the average probabilities of exclusion $P_i^E(\mathbf{A})$ from Eq. (8) (via quasi-Monte Carlo method) is –to the best of our knowledge– the most efficient alternative to compute species-level probabilities of exclusion from a structuralist point of view.

Feasibility domain' shape: Feasibility asymmetry index

Taking into account the features of the average probabilities of exclusion ($P_i^E(\mathbf{A}) \in [0,1]$) and their link with the shape of the feasibility domain, we use a relative Shannon diversity index J', introduced by Pielou (1976), to describe the distribution of the average probabilities of exclusion. This index, which in our context we called "feasibility asymmetry index", is a commonly-used equitability index in ecological studies (Tuomisto, 2012). It has the following three desirable properties: i) it is maximal and equal to one when the average probabilities of exclusion are equal (i.e, when the feasibility domain is symmetric); ii) it approaches zero when the average probabilities of exclusion are very dissimilar; and iii) the index shows values in the middle of its scale when the differences between probabilities can be intuitively considered "intermediate" (see a full description of its features in (Smith & Wilson, 1996)). The feasibility asymmetry index is of the form:

$$J'(\mathbf{A}) = \frac{-\sum_{i=1}^{S} P_i^E(\mathbf{A}) \log\left(P_i^E(\mathbf{A})\right)}{\log(S)}. \tag{9}$$

where S is the total number of species in the community. We use the notation $J'(\mathbf{A})$ to highlight the dependence of the results on the interaction matrix. Since $P_i^E(\mathbf{A})$ depends on the size of the feasibility domain, the latter also affects $J'(\mathbf{A})$. Indeed, given feasibility domains whose sides are proportional, the larger the size of a given domain, the greater the differences among $P_i^E(\mathbf{A})$ and, thus, the more asymmetric (i.e., the smaller $J'(\mathbf{A})$) (see Fig. S6 for an example). Nevertheless, the dependence of $P_i^E(\mathbf{A})$ and $J'(\mathbf{A})$ on size is smaller than that of other shape indices (see Suppl. Fig. S6 for an example).

Theoretical predictions for empirical communities

With the perspective presented above and the associated methodological tools, we can advance our understanding of the feasibility and composition of ecological communities. Yet, because these tools use underlying population models we can additionally predict temporal changes in the abundance of interacting species. Our main prediction is that the asymmetry of species interactions, which can be computed with the above-described shape-based metrics, modulates the population dynamics of

species, and therefore, can inform of temporal change in species abundances, at least at short-term. If that is true, our approach can help predict changes in abundances in species-rich communities while maintaining a mechanistic understanding, which is one of the key challenges in ecology (Ehrlén & Morris, 2015). In particular, our first theoretical expectation is that, the smaller the exclusion ratio (ER_i) or the larger the exclusion distance (θ_i) of a given species, the larger the perturbation needed to exclude such species from the community, and the more likely to have positive growth rates, which will result in larger future abundances (Fig. 3). Complementing this hypothesis, we predict that the more accurate the structural characterization of the community (by providing information of species interactions and their intrinsic growth rates), the better the prediction. That is, we expect that predictions based on detailed structural information, such as the exclusion distances θ_i (extracted from species' intrinsic growth rates at a given time), will perform better than those derived from a probabilistic average, like the exclusion ratios ER_i (Fig. 3).

Empirical information to test our two central predictions in this perspective comes from a long-term observational study in species-rich communities located at a Mediterranean grassland. There, we gathered information on the observed abundances, reproduction rates and interactions between annual plant species during seven years, from 2015 to 2021 (García-Callejas *et al.*, 2021).

Study system

From November 2014 to September 2021, we sampled each year at our experimental site (Caracoles Ranch), located in Doñana National Park, SW Spain (37°04'01.0" N, 6°19'16.2" W), 19 annual species present in the study area, that accounted for $> 90\%$ of plant biomass in the community. These 19 species belong to disparate taxonomic families and exhibit contrasted functional profiles along the growing season (Supplementary table S1). The earliest species with small size and open flowers, such as *Chamaemelum fuscatum* (Asteraceae), peak at beginning of the growing season (February), while late species with succulent leaves, such as *Salsola soda* (Amaranthaceae), grow during summer and peak at the end of the growing season (September-October).

With this experimental setting and following the methodology described in (García-Callejas *et al.*, 2021; Lanuza *et al.*, 2018), we used the plant neighborhoods in relation to individual repro-

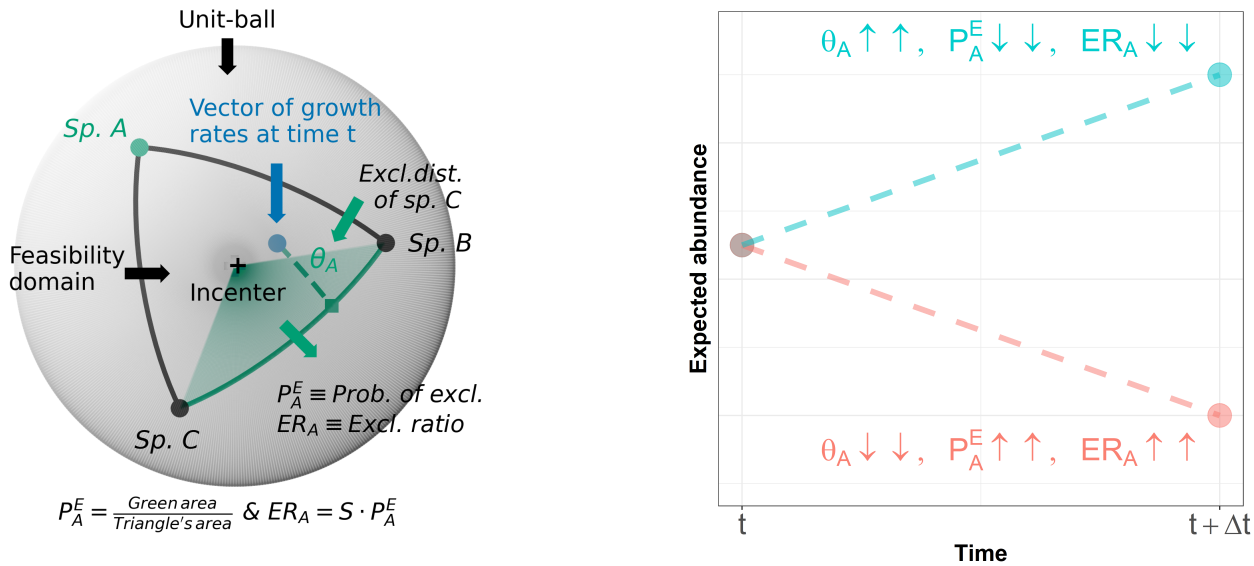

(a) (b)

Fig. 3: (a) Example of the shape-based exclusion metrics that can be estimated for a species that belongs to a (symmetric) community with $S = 3$ species, namely: the exclusion distance of species A (θ_A), its average probability of exclusion (P_A^E) and its corresponding exclusion ratio (ER_A). (b) Expected relationships between the shape-based exclusion metrics of a single species in a given year (t) and its future abundance ($t + \Delta t$).

ductive success to parameterize empirical estimates of intra- and interspecific pairwise plant-plant interactions (i.e., the elements α_{ij} of the interaction matrices $\mathbf{A}$) for each year, along with the annual, intrinsic growth rates of plants (see further details in Suppl. Section 7). Aside from these data, we also recorded annually an independent measure of field abundance for each of the 19 species considered (see Suppl. table S1). The sampling coverage of plant-plant interactions, quantified via rarefaction curves, was $> 99\%$ in all annual communities (Suppl. Section 8).

Estimation of shape-based metrics

Using the empirical estimates of the interaction matrices and intrinsic growth rates, we obtained the annual exclusion distances and the exclusion ratios for the 19 plant species in our system. The former were derived from Eq. (S7), whereas the latter were estimated from Eqs. (4) and (6), by applying the quasi-Monte Carlo estimation of relative volumes (based on Eq. (8)), and generating 10,000 random draws for each required value of exclusion probability, $P_i^E(\mathbf{A})$. For these calculations, we assume that the interaction coefficients and the exclusion metrics represent the

corresponding averaged values within a given year.

Statistical analyses

We analyzed the correlation of the species exclusion ratio ER_i (based only on the interaction structure) and the species exclusion distance θ_i (based on both the interaction structure and the demographic performance) with the observed short-term species abundances in our grassland study system. Note that abundance data is completely independent of the data used to calculate the interaction strengths (see details in (García-Callejas *et al.*, 2021)). Therefore, they provide a rigorous test to evaluate the ability of our metrics to predict the population dynamics of interacting species. Specifically, we fitted three different generalized linear models (GLMs) to the observed data from a given year t, and compared the predicted abundances to the observed abundances at $t+1$. Then, we compared those models on the basis of AIC to asses which model better described the patterns observed (Burnham & Anderson, 2004). For these analyses, given that not all the estimated interaction matrices contained the same pool of plant species, we only used the results for those species that were present from 2015 to 2021. In addition, we did not consider the data of the growing season of 2018 (that is, we did not try to predict the abundances in 2018 from the data in 2017) because that growing season was dominated by the extreme flooding event which does not reflect the annual plant dynamics (see García-Callejas *et al.* (2021) for details on that perturbation and its effects on the community). After applying the above filtering, we selected the abundances, exclusion distances, and exclusion ratios of seven plant species from contrasted taxonomic groups, namely: *Beta macrocarpa*, *Centaurium tenuiflorum*, *Hordeum marinum*, *Leontodon maroccanus*, *Parapholis incurva*, *Polypogon maritimus*, and *Salsola soda*.

Our first statistical (GLM) model (*base model*) used the abundance of a given species in year t and its identity (a categorical variable) to explain its future abundance in year $t+1$. Our second model (*exclusion ratio model*) further considered the exclusion ratio in year t as an additional explanatory variable, whereas our third model (*exclusion distance model*) used the exclusion distance in year t instead of the exclusion ratio. Hence, we assumed that the relevant abiotic and biotic factors that drove the species dynamics during a given year were encoded in our shape-based

metrics (Ehrlén & Morris, 2015). In addition, note that our models did not include information on the dispersal ability of the focal species, but given the nature of the study system which flooded every year, we assume there is no limitation to global dispersal in the study area.

Since our response variables represent count data (number of plant individuals), we used a negative binomial model (with a linear parametrization (Hardin & Hilbe, 2012)) in our inferences with a log link function. Given the limited number of plant species, it is not advised to consider more complex model structures, such as accounting for variation across species explicitly through random effects (Harrison *et al.*, 2018). We, nevertheless, tested generalized linear mixed models with plant species as random effect, which rendered similar trends as the ones reported for our GLMs, but whose residual diagnostics showed problems with the random effect addition.

To keep the regression variables on similar scales and use the fitted parameters of the models as (within-study) effect-sizes, that is, measures of variable importance (Schielzeth, 2010), all numeric explanatory variables were centered and scaled during the analysis. Our analyses were conducted in R, with the `glmmTMB` v1.1.3 package (Brooks *et al.*, 2017). We found no collinearity among explanatory variables when we checked their variance inflation factors with the R-package `performance` v0.8.0 (Lüdecke *et al.*, 2021). We also checked model assumptions with the R-package `DHARMa` v0.4.5 (Hartig, 2022) (see model diagnostics in Suppl. Figs. S13 and S14).

Results

In our seven years of sampling, we documented and parameterized 126 and 2,142 intra- and interspecific pairwise plant-plant interactions, respectively. From them, we extracted 7 annual interaction matrices $\mathbf{A}$, whose average number of species per year was 15.29 ± 3.35. The estimated interaction strengths α_{ij} (the elements of $\mathbf{A}$) were either negative (i.e. denoting competition) or positive (i.e. denoting facilitation). Further, the distribution of the absolute value of α_{ij} was right-skewed throughout all the years, with the bulk of the interactions being weak and very few interactions being strong (see Suppl. Fig. S7). The variation of those asymmetries in interactions strengths, as expected, also exerted changes in the features (size and shape) of the feasibility domain of our communities. That is consistent with the idea that species sensitivity to perturbations

is dependent on the system state and its structure of interactions with other species, as in the case of food webs (Beauchesne *et al.*, 2021) or systems out-of equilibrium (Medeiros *et al.*, 2022). The maximum values of feasibility domain size (Ω) and symmetry (J') were reached from 2016 to 2018 ($\Omega_{\max} = 0.382$ and $J'_{\max} = 0.940$), and the minimum ones in 2019 and 2020 ($\Omega_{\min} = 0.0823$ and $J'_{\max} = 0.478$) being 0.5 and 1 the upper bounds of Ω and J' (see Suppl. Fig. S8).The shape-based metrics for the pool of species that was present throughout all the sampling years revealed that, in general, the vulnerability of species to exclusion, expressed via species exclusion ratios and exclusion distances (Box 1, 3(a)), fluctuates across years (see Suppl. Figs. S9, S10 and Suppl. Fig. S11).

Results from our GLMs supported our theoretical expectations. On the one hand, statistical outputs confirmed that the exclusion ratios exerted a negative influence on the number of individuals found next year in our study site (effect-size: -0.57, see table S4). That is, those species that have larger probabilities of exclusion reduced their population the following year. Conversely, the exclusion distances have a positive effect on population abundance (effect-size: 0.41, see table S5) indicating that those species that were further away from the edge of the feasibility domain increased their population the following year. Another important finding is that the effect size of the abundance in the previous year is three to 75 times smaller than those of the exclusion ratio and exclusion distance, respectively. In line with this finding, predictions based on detailed structural information performed better than those based solely on previous abundances. Specifically, we found that the model including the exclusion distance as an explanatory variable is the one that better describes the data (see Suppl. table S6), since it shows the lowest AIC obtained among the set of models examined ($\mathrm{AIC}_{\min}$). Taken together, these results suggests that the population abundance in the previous year have little influence in the abundance of the next year compared to the effect of species interactions and intrinsic growth rates.

Finally, we also found that the intercept for *Hordeum marinum* and *Leontodon maroccanus*, the most abundant species (Supplementary table S1), are positive (effect-sizes > 9, see tables S3, S4 and S5). This result indicates that the prediction of future population abundances is easier when species are relatively more common than rare (see a comparison between observed and predicted

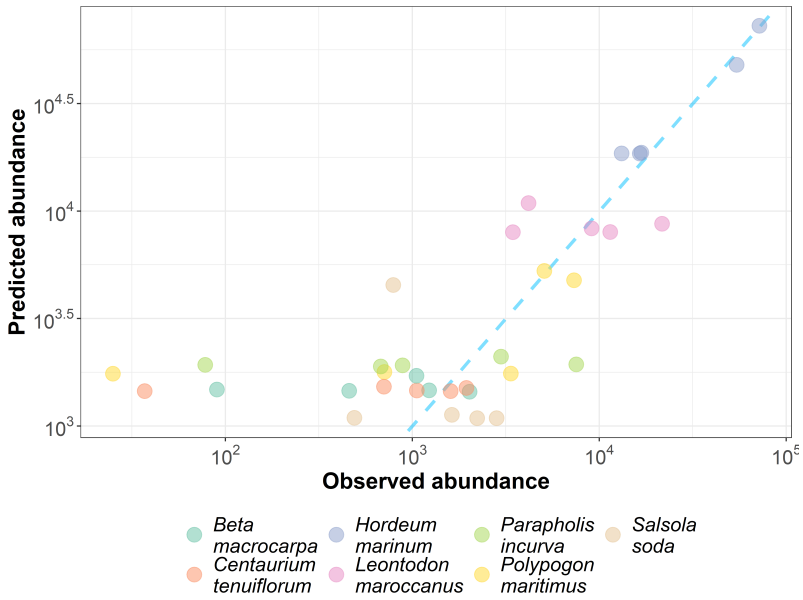

Fig. 4: Predicted versus observed abundances for the pool of 7 species selected in Caracoles Ranch ($N = 35$ observations), when using the exclusion distance model (see fit details in table S6). The set of points for each species corresponds to the forecast of the following years: 2015-16, 2016-17, 2018-19, 2019-20, and 2020-21. As described in the main text, we did not consider predictions for 2018 due to the large-scale external perturbation of the plant dynamics that year. The blue dashed line is a guide to the eye that locates predictions that are equal to the observed values. Note that the four points visually deviating from the dashed line represent small deviations which appear visually amplified in the logarithmic scale.

abundances in Fig. 4).

Box 2 — Assessing exclusion risks in mutualistic communities with shape-based metrics: A proof of concept.

The structure of plant-pollinator interactions can encapsulate information about the sensitivity of different species to perturbations. For example, there is considerable evidence supporting the relationship between specialization and extinction risk (Bartomeus *et al.*, 2013; Biella *et al.*, 2020; Burkle *et al.*, 2013; Memmott *et al.*, 2007; Scheper *et al.*, 2014): extinction risk declines with increasing numbers of mutualist partners, from least-linked (most specialized) species to most-linked (most generalized) ones.

Here we test if the ranking of our shape-based metrics, which quantify the species' average probability of being the first species excluded from a given community, aligns with the expected relationship between specialization and extinction risk described in the literature. To do

so, first, we extracted from the Mangal database (Poisot *et al.*, 2016) 88 empirical plant-pollinator networks from 5 different studies with wide geographical coverage (see details in table S7). Such data comprises 1,734 species in total, where 1,198 species were animals. On average each network had 19.70 ± 9.18 nodes of which 13.61 ± 6.94 were animals. For each of these networks, we estimated the communities' effective interaction matrices by using the mean field approximation for intra-guild competition and the two inter-guild parameterizations proposed in (Saavedra *et al.*, 2016b) for mutualistic communities. Then, we extracted the species' average probability of exclusion, $P_i^E(\mathbf{A})$, by using Eq. (8). We quantify probabilities of exclusion instead of exclusion distances because we lack estimations of intrinsic growth rates in these 88 communities.

In Fig. 5 we show the results of this analysis for a particular network: overall, least-linked species exhibit a larger probability of exclusion than most-linked ones. Further, we observe that most pollinators are at more immediate risk of exclusion than plants, which is congruent with previous empirical and theoretical findings (Biella *et al.*, 2020; Memmott *et al.*, 2004). Such trends were consistent across networks and mean-field approaches (see Suppl. Figs. S15 and S16). Analyses based on structural, probabilistic metrics, can therefore be useful in different contexts, including the comparison of species or community-level trends across environmental or geographical gradients, or studies aiming to pinpoint potential species of conservation interest.

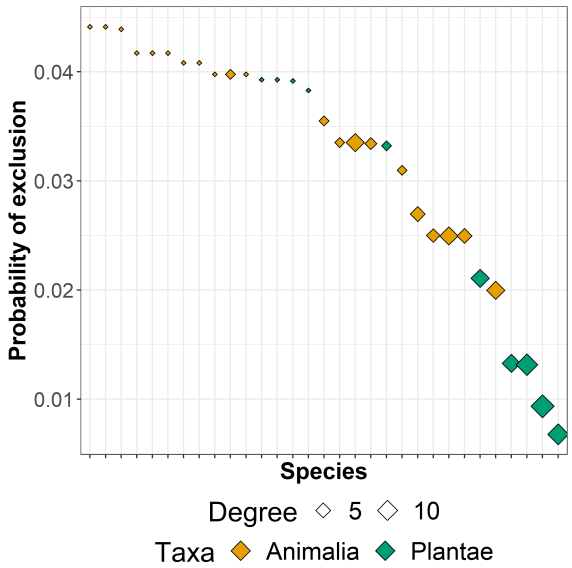

Fig. 5: Average probability of exclusion, $P_i^E(\mathbf{A})$ [Eq. (8)], for a mutualistic network in Bartomeus *et al.* (2008) with $S = 31$ species (21 insect and 10 plant nodes, respectively), extracted from the Mangal database (Poisot *et al.*, 2016). To create the interaction matrix, we followed the mean field approximation for intra-guild competition and the two inter-guild parameterizations in (Saavedra *et al.*, 2016b) for systems with no interspecific competition, namely: $\rho = 0.00$, $\delta = 0.25$ and $\gamma_0 = 0.50\,\langle\gamma_{ij}\rangle$ (see further details on the parameters in the referred paper). The color and the size of markers show the node's taxa and degree, respectively. Note that for this particular network the authors sampled all plants with an equal sampling effort, hence, plant abundance is not confounded with a larger sampling effort, which may lead to detecting more links, and inflating the degree of abundant plants.

Discussion

A central theme in ecology is which information we need to mechanistically understand and predict the vulnerability of species to perturbations coming, for example, from environmental changes. This question can be approached from different angles: from looking at physiological tolerances to different environmental stressors, to analyzing species' demographic vital rates, or to exploring the joint response of species interacting with each other. In this perspective, we show that adopting a community context, supported by a reliable quantification of species interactions, is critical to predict the effect of environmental perturbations on the persistence of both particular species and entire communities. The joint possibility of keeping a mechanistic understanding of how biodiversity is maintained across ecological levels of organization while achieving a good predictive power is now possible by acknowledging the idea that species present in natural systems show

asymmetries in their biotic interaction, and, therefore, the size and the shape of the feasibility domain should be simultaneously explored.

A remarkable finding is that the shape-based metrics developed here are useful to predict changes in population abundances from one year to another among interacting species in a grassland system (see table S6). This is a strong result taking into account that the studied species are annual plants whose abundances depend on a myriad of factors, including inter-annual variation in rainfall and temperature, demographic processes such as individual fecundity, germination rates, and seed survival in the soil bank, as well as interactions with other competitors, pollinators, mycorrhizae, and natural enemies. Overall, these results suggest that, although simplistic, the structure of species interactions and species' demographic performance phenomenologically capture key ingredients of the processes controlling population dynamics and are more meaningful for making predictions that just considering abundances from previous years. In our particular case, the best predictive model was the one that included information on the demographic performance and species interactions (i.e., exclusion distances) compared to the model based only on probabilistic averages extracted from species interactions (i.e., exclusion ratios). These results agree with our original hypothesis that including more biological information would improve predictions (Daugaard *et al.*, 2022; Petchey *et al.*, 2015a). Another important result of this perspective is that our shape-based metrics do not display the same predictive power across species. In particular, we have found that the most abundant plant species in our system (*Hordeum marinum* and *Leontodon maroccanus*, see Suppl. table S1 and Fig. 4), were easier to predict than others (see table S5). These findings suggest that the structure of species interactions might not be meaningful to predict abundances of rare species in a given community, but further research is needed to explore this possibility. Overall, these results reinforce the idea that increasing system complexity its not incompatible with the predictability of the dynamics of its components (Daugaard *et al.*, 2022). Rather, our results emphasize that a combination of the interaction structure of the system and species-level properties, such as demographic performance, balance the ability to predict species outcomes. As shown in Box 2, this framework can accommodate more complex communities considering not only plants but also, for example, plant-pollinator systems. Empirically documenting

all relevant competitive, mutualistic and trophic interactions of a community is the next step needed to enrich the modelling process.

The metrics we propose here integrating species-level sensitivity to perturbations (i.e. the range of reproductive outcomes that lead to species persistence) within a community-level measure of feasibility (i.e. the *feasibility asymmetry index*) do not start from scratch. They rather build on previous efforts (Grilli *et al.*, 2017; Tabi *et al.*, 2020) that identified a key issue in the structuralist approach: the size of the feasibility domain, by itself, is not fully representative of the capacity of a community to withstand perturbations. Rather, we need to quantify its shape, i.e. the relative contribution of each species to it. Both properties are not fully independent in spherical geometry, which is the mathematical backbone of the structuralist approach (Suppl. Section 1). However, just like we might expect for two proportional triangles in two-dimensional geometry to have the same "shape" according to a quantifiable metric, we might approach that intuitive requirement in spherical geometry. Our feasibility asymmetry index fulfills this requirement more robustly than previous approaches, i.e. it's much less sensitive to variations in the size of the feasibility domain for a given shape (Fig. S6). We provide implementations of all the metrics discussed here in the R package `anisoFun` v1.0: `https://github.com/RadicalCommEcol/anisoFun`, and we suggest that their adoption may help bridge the gap between ecological theory and empirical studies, in order to provide new solutions to manage, conserve and restore biodiversity thanks to their predictive power. For instance, highly asymmetric feasibility domains due to high asymmetries in biotic interactions among members of an ecological community are indicative of strong differences in species probabilities of exclusion, which can be used as an indicator, in applied contexts, that detailed analyses of extinction risk are necessary. On the contrary, such additional risk analyses would not be so critical to perform in symmetric feasibility domains, where all species have a similar probability of exclusion.

The applicability of these metrics for a wide range of systems and community types remains an open question, but we can anticipate some limitations. On the theoretical side, we assume that the basic elements contained in the structure of species interactions (i.e., pairwise interactions) varies across years but can be well-approximated by annually-averaged values within a given year, and

that functional forms (i.e. the relationship between species abundances and overall interaction effects) are linear. However, the existence of non-linear functional forms for modeling pairwise interactions (or even the addition of higher-order interactions as in (Gibbs *et al.*, 2022)) will have non-trivial consequences on system dynamics (Dougoud *et al.*, 2018), and may preclude the use of the linear definition of the feasibility domain that sustains our approach. This framework is, nevertheless, able to accommodate different types of interactions beyond plant-plant interactions (Box 2), as well as alternative functional forms and dynamics (such as those of the saturating competition model by Brauer & Castillo-Chavez (2011) and other examples in (Cenci & Saavedra, 2018; Saavedra *et al.*, 2017)). On the empirical side, it is premature to generalize these results to other systems because the importance of obtaining robust demographic performance data and the predictive skill gained with it is likely to be context-dependent. For instance, a single demographic performance value might not be as meaningful for systems with more complex life cycles. Overall, we argue that the toolbox developed here is ready to be used for systems whose species display similar population dynamics and similar responses to external perturbations (e.g. annual plant communities, coral reef fishes, tropical trees, plant-pollinator mutualistic systems) (Box 2, García-Callejas *et al.* (2023)).

Conclusion

Reliable tools for predicting ecological outcomes remain elusive and, in general, disconnected from those frameworks used to understand ecological processes. Here we provide a novel set of metrics within a structuralist approach that considers the conditions leading to the persistence of species and entire ecological systems. This consideration stems from the fact that biotic interactions among species are as a general rule asymmetric in their strength and sign within ecological communities. Our aim is to advance in unifying our mechanistic understanding of the maintenance of biodiversity in ecological communities while simultaneously increasing the predictive ability of their dynamics. We have shown that including information on species interactions and their demographic performance in the estimation of these shape-based structural metrics significantly improves short-term forecasts of species abundances in an annual plant community, compared to

forecasts based only on species' previous abundances. The species and community-level metrics presented here are general across interaction types and can be efficiently obtained for communities of arbitrary richness, unlocking the possibility of systematically studying the biotic control over ecological dynamics for a wide range of systems.

Bibliography

Adler, P. B., Smull, D., Beard, K. H., Choi, R. T., Furniss, T., Kulmatiski, A., Meiners, J. M., Tredennick, A. T. & Veblen, K. E. (2018). Competition and coexistence in plant communities: intraspecific competition is stronger than interspecific competition. *Ecology letters*, 21, 1319–1329.

Bartomeus, I., Park, M. G., Gibbs, J., Danforth, B. N., Lakso, A. N. & Winfree, R. (2013). Biodiversity ensures plant-pollinator phenological synchrony against climate change. *Ecol. Lett.*, 16, 1331–1338.

Bartomeus, I., Saavedra, S., Rohr, R. P. & Godoy, O. (2021). Experimental evidence of the importance of multitrophic structure for species persistence. *Proc. Natl. Acad. Sci. U. S. A.*, 118, e2023872118.

Bartomeus, I., Vilà, M. & Santamaría, L. (2008). Contrasting effects of invasive plants in plant-pollinator networks. *Oecologia*, 155, 761–770.

Bascompte, J., Jordano, P. & Olesen, J. M. (2006). Asymmetric coevolutionary networks facilitate biodiversity maintenance. *Science*, 312, 431–433.

Beauchesne, D., Cazelles, K., Archambault, P., Dee, L. E. & Gravel, D. (2021). On the sensitivity of food webs to multiple stressors. *Ecol. Lett.*, 24, 2219–2237.

Biella, P., Akter, A., Ollerton, J., Nielsen, A. & Klecka, J. (2020). An empirical attack tolerance test alters the structure and species richness of plant–pollinator networks. *Funct. Ecol.*, 34, 2246–2258.

Bimler, M. D., Stouffer, D. B., Lai, H. R. & Mayfield, M. M. (2018). Accurate predictions of coexistence in natural systems require the inclusion of facilitative interactions and environmental dependency. *Journal of Ecology*, 106, 1839–1852.

Brauer, F. & Castillo-Chavez, C. (2011). *Mathematical models in population biology and epidemiology*. Texts in Applied Mathematics, 2nd edn. Springer, New York, NY.

Brooks, M. E., Kristensen, K., van Benthem, K. J., Magnusson, A., Berg, C. W., Nielsen, A., Skaug, H. J., Maechler, M. & Bolker, B. M. (2017). glmmTMB balances speed and flexibility among packages for zero-inflated generalized linear mixed modeling. *The R Journal*, 9, 378–400.

Burkle, L. A., Marlin, J. C. & Knight, T. M. (2013). Plant-pollinator interactions over 120 years: loss of species, co-occurrence, and function. *Science*, 339, 1611–1615.

Burnham, K. P. & Anderson, D. R. (2004). Multimodel inference. *Sociol. Methods Res.*, 33, 261–304.

Cenci, S. & Saavedra, S. (2018). Structural stability of nonlinear population dynamics. *Phys. Rev. E.*, 97.

Cenci, S., Song, C. & Saavedra, S. (2018). Rethinking the importance of the structure of ecological networks under an environment-dependent framework. *Ecol. Evol.*, 8, 6852–6859.

Civantos-Gómez, I., García-Algarra, J., García-Callejas, D., Galeano, J., Godoy, O. & Bartomeus, I. (2021). Fine scale prediction of ecological community composition using a two-step sequential machine learning ensemble. *PLOS Computational Biology*, 17, e1008906.

Clark, A. T., Ann Turnbull, L., Tredennick, A., Allan, E., Harpole, W. S., Mayfield, M. M., Soliveres, S., Barry, K., Eisenhauer, N., de Kroon, H. *et al.* (2020). Predicting species abundances in a grassland biodiversity experiment: Trade-offs between model complexity and generality. *Journal of ecology*, 108, 774–787.

Daugaard, U., Munch, S. B., Inauen, D., Pennekamp, F. & Petchey, O. L. (2022). Forecasting in the face of ecological complexity: Number and strength of species interactions determine forecast skill in ecological communities. *Ecol. Lett.*

Dietze, M. C. (2017). Prediction in ecology: A first-principles framework. *Ecological Applications*, 27, 2048–2060.

Dougoud, M., Vinckenbosch, L., Rohr, R. P., Bersier, L.-F. & Mazza, C. (2018). The feasibility of equilibria in large ecosystems: A primary but neglected concept in the complexity-stability debate. *PLoS Comput. Biol.*, 14, e1005988.

Ehrlén, J. & Morris, W. F. (2015). Predicting changes in the distribution and abundance of species under environmental change. *Ecology Letters*, 18, 303–314.

Evans, J. S., Murphy, M. A., Holden, Z. A. & Cushman, S. A. (2011). Modeling species distribution and change using random forest. In: *Predictive species and habitat modeling in landscape ecology*. Springer, pp. 139–159.

García-Callejas, D., Bartomeus, I. & Godoy, O. (2021). The spatial configuration of biotic interactions shapes coexistence-area relationships in an annual plant community. *Nature Communications*, 12.

García-Callejas, D., Godoy, O., Buche, L., Hurtado, M., Lanuza, J. B., Allen-Perkins, A. & Bartomeus, I. (2023). Non-random interactions within and across guilds shape the potential to coexist in multi-trophic ecological communities. *Ecology Letters*, in press.

Genz, A. & Bretz, F. (2009). *Computation of Multivariate Normal and t Probabilities*. Lecture notes in statistics, 2009th edn. Springer, Berlin, Germany.

Genz, A., Bretz, F., Miwa, T., Mi, X., Leisch, F., Scheipl, F. & Hothorn, T. (2021). *mvtnorm: Multivariate Normal and t Distributions*. URL `https://CRAN.R-project.org/package=mvtnorm`. R package version 1.1-2.

Gibbs, T., Levin, S. A. & Levine, J. M. (2022). Coexistence in diverse communities with higher-order interactions. *Proc. Natl. Acad. Sci. U. S. A.*, 119, e2205063119.

Godoy, O., Bartomeus, I., Rohr, R. P. & Saavedra, S. (2018). Towards the integration of niche and network theories. *Trends in Ecology & Evolution*, 33, 287–300.

Godoy, O. & Levine, J. M. (2014). Phenology effects on invasion success: Insights from coupling field experiments to coexistence theory. *Ecology*, 95, 726–736.

Gourion, D. & Seeger, A. (2010). Deterministic and stochastic methods for computing volumetric moduli of convex cones. *Computational & Applied Mathematics*, 29.

Grilli, J., Adorisio, M., Suweis, S., Barabás, G., Banavar, J. R., Allesina, S. & Maritan, A. (2017). Feasibility and coexistence of large ecological communities. *Nature Communications*, 8.

Hardin, J. W. & Hilbe, J. M. (2012). *Generalized linear models and extensions, third edition*. 3rd edn. Stata Press, Philadelphia, PA.

Harrison, X. A., Donaldson, L., Correa-Cano, M. E., Evans, J., Fisher, D. N., Goodwin, C. E. D., Robinson, B. S., Hodgson, D. J. & Inger, R. (2018). A brief introduction to mixed effects modelling and multi-model inference in ecology. *PeerJ*, 6, e4794.

Hart, S. P., Freckleton, R. P. & Levine, J. M. (2018). How to quantify competitive ability. *J. Ecol.*, 106, 1902–1909.

Hartig, F. (2022). *DHARMa: Residual Diagnostics for Hierarchical (Multi-Level / Mixed) Regression Models*. URL `https://CRAN.R-project.org/package=DHARMa`. R package version 0.4.5.

Lanuza, J. B., Bartomeus, I. & Godoy, O. (2018). Opposing effects of floral visitors and soil conditions on the determinants of competitive outcomes maintain species diversity in heterogeneous landscapes. *Ecology Letters*, 21, 865–874.

Levine, J. M., Bascompte, J., Adler, P. B. & Allesina, S. (2017). Beyond pairwise mechanisms of species coexistence in complex communities. *Nature*, 546, 56–64.

Logofet, D. O. (2005). Stronger-than-Lyapunov notions of matrix stability, or how "flowers" help solve problems in mathematical ecology. *Linear Algebra Appl.*, 398, 75–100.

Lüdecke, D., Ben-Shachar, M. S., Patil, I., Waggoner, P. & Makowski, D. (2021). performance: An R package for assessment, comparison and testing of statistical models. *Journal of Open Source Software*, 6, 3139.

MacArthur, R. H. (1957). On the relative abundance of bird species. *Proceedings of the National Academy of Sciences*, 43, 293–295.

McGill, B. J., Etienne, R. S., Gray, J. S., Alonso, D., Anderson, M. J., Benecha, H. K., Dornelas, M., Enquist, B. J., Green, J. L., He, F., Hurlbert, A. H., Magurran, A. E., Marquet, P. A., Maurer, B. A., Ostling, A., Soykan, C. U., Ugland, K. I. & White, E. P. (2007). Species abundance distributions: Moving beyond single prediction theories to integration within an ecological framework. *Ecology Letters*, 10, 995–1015.

Medeiros, L. P., Allesina, S., Dakos, V., Sugihara, G. & Saavedra, S. (2022). Ranking species based on sensitivity to perturbations under non-equilibrium community dynamics.

Memmott, J., Craze, P. G., Waser, N. M. & Price, M. V. (2007). Global warming and the disruption of plant-pollinator interactions. *Ecol. Lett.*, 10, 710–717.

Memmott, J., Waser, N. M. & Price, M. V. (2004). Tolerance of pollination networks to species extinctions. *Proc. Biol. Sci.*, 271, 2605–2611.

Peñuelas, J., Canadell, J. G. & Ogaya, R. (2011). Increased water-use efficiency during the 20th century did not translate into enhanced tree growth. *Glob. Ecol. Biogeogr.*, 20, 597–608.

Petchey, O. L., Pontarp, M., Massie, T. M., Kéfi, S., Ozgul, A., Weilenmann, M., Palamara, G. M., Altermatt, F., Matthews, B., Levine, J. M., Childs, D. Z., McGill, B. J., Schaepman, M. E., Schmid, B., Spaak, P., Beckerman, A. P., Pennekamp, F. & Pearse, I. S. (2015a). The ecological forecast horizon, and examples of its uses and determinants. *Ecol. Lett.*, 18, 597–611.

Petchey, O. L., Pontarp, M., Massie, T. M., Kéfi, S., Ozgul, A., Weilenmann, M., Palamara, G. M., Altermatt, F., Matthews, B., Levine, J. M., Childs, D. Z., McGill, B. J., Schaepman, M. E., Schmid, B., Spaak, P., Beckerman, A. P., Pennekamp, F. & Pearse, I. S. (2015b). The ecological forecast horizon, and examples of its uses and determinants. *Ecology Letters*, 18, 597–611.

Pielou, E. C. (1976). *Ecological Diversity.* John Wiley & Sons, Nashville, TN.

Poisot, T., Baiser, B., Dunne, J. A., Kéfi, S., Massol, F., Mouquet, N., Romanuk, T. N., Stouffer, D. B., Wood, S. A. & Gravel, D. (2016). Mangal – making ecological network analysis simple. *Ecography*, 39, 384–390.

Saavedra, S., Medeiros, L. P. & AlAdwani, M. (2020). Structural forecasting of species persistence under changing environments. *Ecology Letters*, 23, 1511–1521.

Saavedra, S., Rohr, R. P., Bascompte, J., Godoy, O., Kraft, N. J. & Levine, J. M. (2017). A structural approach for understanding multispecies coexistence. *Ecological Monographs*, 87, 470–486.

Saavedra, S., Rohr, R. P., Fortuna, M., Selva, N. & Bascompte, J. (2015). Seasonal species interactions minimize the impact of species turnover on the likelihood of community persistence. *Ecology.*

Saavedra, S., Rohr, R. P., Olesen, J. M. & Bascompte, J. (2016a). Nested species interactions promote feasibility over stability during the assembly of a pollinator community. *Ecol. Evol.*, 6, 997–1007.

Saavedra, S., Rohr, R. P., Olesen, J. M. & Bascompte, J. (2016b). Nested species interactions

promote feasibility over stability during the assembly of a pollinator community. *Ecology and Evolution*, 6, 997–1007.

Scheper, J., Reemer, M., van Kats, R., Ozinga, W. A., van der Linden, G. T. J., Schaminée, J. H. J., Siepel, H. & Kleijn, D. (2014). Museum specimens reveal loss of pollen host plants as key factor driving wild bee decline in the netherlands. *Proc. Natl. Acad. Sci. U. S. A.*, 111, 17552–17557.

Schielzeth, H. (2010). Simple means to improve the interpretability of regression coefficients. *Methods in Ecology and Evolution*, 1, 103–113.

Shoemaker, L. G., Sullivan, L. L., Donohue, I., Cabral, J. S., Williams, R. J., Mayfield, M. M., Chase, J. M., Chu, C., Harpole, W. S., Huth, A., HilleRisLambers, J., James, A. R. M., Kraft, N. J. B., May, F., Muthukrishnan, R., Satterlee, S., Taubert, F., Wang, X., Wiegand, T., Yang, Q. & Abbott, K. C. (2019). Integrating the underlying structure of stochasticity into community ecology. *Ecology*, 101, e02922.

Smith, B. & Wilson, J. B. (1996). A consumer's guide to evenness indices. *Oikos*, 76, 70.

Song, C., Rohr, R. P. & Saavedra, S. (2018). A guideline to study the feasibility domain of multi-trophic and changing ecological communities. *Journal of Theoretical Biology*, 450, 30–36.

Song, C., Von Ahn, S., Rohr, R. P. & Saavedra, S. (2020). Towards a probabilistic understanding about the context-dependency of species interactions. *Trends Ecol. Evol.*, 35, 384–396.

Tabi, A., Pennekamp, F., Altermatt, F., Alther, R., Fronhofer, E. A., Horgan, K., Mächler, E., Pontarp, M., Petchey, O. L. & Saavedra, S. (2020). Species multidimensional effects explain idiosyncratic responses of communities to environmental change. *Nature Ecology and Evolution*, 4, 1036–1043.

Tredennick, A. T., Hooker, G., Ellner, S. P. & Adler, P. B. (2021). A practical guide to selecting models for exploration, inference, and prediction in ecology. *Ecology*, 102, e03336.

Tredennick, A. T., Hooten, M. B. & Adler, P. B. (2017). Do we need demographic data to forecast plant population dynamics? *Methods in Ecology and Evolution*, 8, 541–551.

Tuomisto, H. (2012). An updated consumer's guide to evenness and related indices. *Oikos*, 121, 1203–1218.

Venturelli, O. S., Carr, A. C., Fisher, G., Hsu, R. H., Lau, R., Bowen, B. P., Hromada, S., Northen, T. & Arkin, A. P. (2018). Deciphering microbial interactions in synthetic human gut microbiome communities. *Mol. Syst. Biol.*, 14, e8157.

Data and code availability

The data and code used to generate the results of this study are available at `https://github.com/RadicalCommEcol/Asymmetric_Interactions`.

Acknowledgements

We thank the Radical Community Ecology group (`https://github.com/RadicalCommEcol/`) for the fruitful discussions. AA-P, DGC, IB and OG were funded by the Spanish Ministry of Science and Innovation (MICINN) and the European Social fund through the MeDiNaS (RTI2018-098888-A-I00), TASTE (PID2021-127607OB-I00), and ChaSisCOMA (PID2021-122711NB-C21) projects. Additionally, OG acknowledges financial support provided by the Spanish Ministry of Economy and Competitiveness (MINECO) and by the European Social Fund through the Ramón y Cajal Program (RYC2017-23666).

Supplementary Material

Title: Structural asymmetry in biotic interactions as a tool to understand and forecast ecological persistence.

Authors: Allen-Perkins, A., García-Callejas, D., Bartomeus, I., Godoy, O.

This document contains the following Supplementary Sections: "Dependence of shape on size for feasibility domains", "Calculation of the incenter and the maximum isotropic perturbation for a given feasibility domain", "Calculation of the exclusion distance of a given species", "Estimation of the probabilities of exclusion via simulations of LV dynamics and shape-based calculations"(Supplementary figures S3-S5), "Testing the dependence of the feasibility asymmetry index on size" (Supplementary figure S6), "Species information for the empirical example in Caracoles Ranch" (Supplementary tables S1-S2 and Supplementary figures S7-S11), "Estimation of the intrinsic growth rates for plant-plant interactions in Caracoles Ranch (Spain)", "Sampling coverage of Caracoles Ranch (Spain)"(Supplementary figure S12), "Results and diagnostics for Caracoles Ranch models" (Supplementary tables S3-S6 and Supplementary figures S13-S14), and "Results for bipartite plant-pollinator networks in Mangal" (Supplementary table S7 and Supplementary figures S15-S16).

1 Dependence of shape on size for feasibility domains

To illustrate the relation between shape and size when characterizing feasibility domains, here we review a counterexample that shows that the independence of both features is false.

Let us consider the simple case of communities with $S = 3$ species. As shown in Fig. 1, in such communities the spaces of growth rates can be represented by an sphere and the growth rates of stable coexistence (feasibility domains) by points that lie within spherical triangles. The border of those triangles limits the corresponding feasibility domains.

To highlight the relation between shape and size of feasibility domains with $S = 3$, let us now consider the area of a spherical triangle with angles α, β, and γ (measured in radians at the vertices, along the surface of the sphere). It is given by

$$\text{Area} = R^2 \left(\alpha + \beta + \gamma - \pi\right) = R^2 E, \tag{S1}$$

where R is the radius of the sphere, and E is called the spherical excess. In the case of spheres with $R = 1$ (like the ones considered in this paper), we can verify that tiny feasible domains (that is, feasible domains where Area $\to 0$) behave like planar triangles (where $E \to 0$) that meet the well-known relation: $\alpha + \beta + \gamma \to \pi$. However, if their area is large, then $\alpha + \beta + \gamma > \pi$. As an example, consider the case of a symmetrical feasible domain, where $\alpha = \beta = \gamma$ (see Fig. S1). According to Eq. (S1), if $R = 1$, then $\alpha = (\text{Area} + \pi)/3$. When Area $\to 0$ our feasible domain looks like a planar equilateral triangle ($\alpha = \pi/3$), whereas if its area is equal to one eighth of that of a full sphere (i.e., Area $= \pi/2$), then our equilateral triangle is an octant of a sphere ($\alpha = \pi/2$). That simple example shows that shape is not independent from size in spherical geometry.

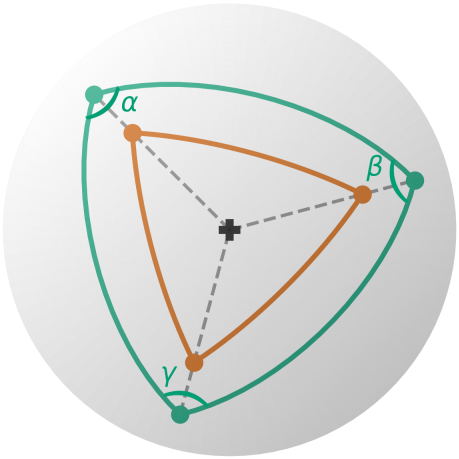

Fig. S1: An example of equilateral spherical triangles. Continuous lines show the border of the respective triangles, grey dashed lines represent the segments of great circles that connect their incenter (black plus marker) with the vertices of the triangles (orange and green dots, respectively). The area of the green triangle is 1.571 square units and their angles are equal to $\pi/2$ radians, whereas the area of the smaller triangle is 0.511 square units and their angles are $2\pi/5$ radians.

2 Calculation of the incenter and the maximum isotropic perturbation for a given feasibility domain

Let us consider a community with S species and an interaction matrix $\mathbf{A}$, that follows Eq. (1). To determine the maximum hyper-spherical cap $\kappa(\mathbf{A})$ that is tangent to all the sides of the feasibility domain's border and whose apex is the incenter $\mathfrak{I}$, we need to know the S vertices and edges ε^S_{S-1} (sections of great circles) that delimit the intersection of the feasibility domain with the unit-ball in S-dimensions, where ε^S_{S-1} denotes the $S-1$-combination of a set S. Firstly, we define vertex V_i as the point on the unit-ball where $N^*_i > 0$ and $N^*_j = 0$ for $j \neq i$. The structural vector $\mathbf{r}$ for vertex V_i can be calculated as $\mathbf{v}_i = \mathbf{u}_i / \|\mathbf{u}_i\|$, where $\mathbf{u}_i = -\mathbf{A}\mathbf{e}_i$, $\mathbf{e}_i$ is a column vector whose i-th component is equal to 1 and the rest are 0, and $\|\mathbf{x}\| = \sqrt{x_1^2 + \cdots + x_S^2}$ represents the Euclidean norm of $\mathbf{x}$. Once we obtained the vertices of the feasibility domain, it is possible to derive the normal direction of the hyper-planes that contain the spherical borders of the feasibility domain, $\mathbf{n}_i$. To calculate the normal vectors $\mathbf{n}_i$, we use the generalization for the cross product in S dimensions of $S-1$ vectors, which produces a vector that is perpendicular to those $S-1$ vectors. Here, we can express $\mathbf{n}_i$ as $\mathbf{n}_i = \mathbf{m}_i / \|\mathbf{m}_i\|$, where:

$$\mathbf{m}_i = \bigwedge_{\substack{k \neq i \\ k \in \{1, \cdots, S\}}} \mathbf{v}_k = \begin{vmatrix} v_1^1 & \cdots & v_1^S \\ \vdots & \ddots & \vdots \\ v_{S-1}^1 & \cdots & v_{S-1}^S \\ \mathbf{e}_1 & \cdots & \mathbf{e}_S \end{vmatrix}. \tag{S2}$$

Since normal vectors have 2 possible orientations, to place the incenter in the feasibility domain, for the normal vectors $\mathbf{n}_i$ we select the orientation that meets the condition $\mathbf{v}_i \cdot \mathbf{n}_j = \sum_{k=1}^S v_i^k n_j^k > 0$ for $i, jk \in \{1, \cdots, S\}$.

By using the normal vectors $\mathbf{n}_i$ calculated above, the incenter $\mathfrak{I}$ and its great circle distance to the boundary of the feasibility domain θ (denoted in the main text as the maximum isotropic perturbation) satisfy the following condition:

$$\begin{pmatrix} \mathbf{n}_1 \\ \hline \vdots \\ \hline \mathbf{n}_S \end{pmatrix} \mathfrak{I} = \begin{pmatrix} n_1^1 & \cdots & n_1^S \\ \vdots & \ddots & \vdots \\ n_S^1 & \cdots & n_S^S \end{pmatrix} \mathfrak{I} = \sin\theta \begin{pmatrix} 1 \\ \vdots \\ 1 \end{pmatrix}, \tag{S3}$$

which is given by the geometrical construction depicted in Fig. S2. Since $\mathfrak{I} \cdot \mathfrak{I} = 1$, and

$$\mathfrak{I} = \sin\theta \begin{pmatrix} n_1^1 & \cdots & n_1^S \\ \vdots & \ddots & \vdots \\ n_S^1 & \cdots & n_S^S \end{pmatrix}^{-1} \begin{pmatrix} 1 \\ \vdots \\ 1 \end{pmatrix}, \tag{S4}$$

the exact values of $\mathfrak{I}$ and θ can be obtained.

In addition, the position of a tangent point shared between the spherical cap (whose incenter is $\mathfrak{I}$) and the border of the FD located in the plane with normal vector $\mathbf{n}_i$, denoted as $\mathbf{T}_i$ (see Supplementary Fig. S2), can be calculated as $\mathbf{T}_i = \mathfrak{I} - \sin(\theta)\mathbf{n}_i$. The tangent point formula is derived by finding the point on the plane with normal vector $\mathbf{n}_i$ whose great circle distance to $\mathfrak{I}$ is θ. That means that the Euclidean distance d from $\mathfrak{I}$ to $\mathbf{T}_i$ is

$$d = \sqrt{\sum_{k=1}^{S} (I_k - T_{i,k})} = \sqrt{2 - 2\cos(\theta)}, \tag{S5}$$

where I_k and $T_{i,k}$ represent the k-th component of $\mathfrak{I}$ and $\mathbf{T}_i$, respectively. Then, the components of $\mathbf{T}_i$ can be obtained by minimizing the function $f(\mathbf{T}_i) = d^2 - 2 + 2\cos(\theta)$ subject to the equality constraint $\mathbf{T}_i \cdot \mathbf{n}_i = 0$, with the method of the Lagrange multipliers.

Finally, note that it is possible to calculate the relative volume of the unit-ball covered by the spherical cap that is tangent to all the sides of the feasibility domain's border and whose apex is the incenter $\mathfrak{I}$ (see blue spherical caps in Fig. 1). That relative volume is given by:

$$\Xi(\mathbf{A}) = \frac{\text{area}\,(\kappa(\mathbf{A}))}{\text{area}\,(B^S)} = \frac{1}{2} I_{\sin^2\theta}\left(\frac{S-1}{2}, \frac{1}{2}\right), \tag{S6}$$

where $I_z\,(a, b)$ is the regularized incomplete beta function (Li, 2010). That relative volume can be used to compare the level of asymmetry between communities with the same number of species

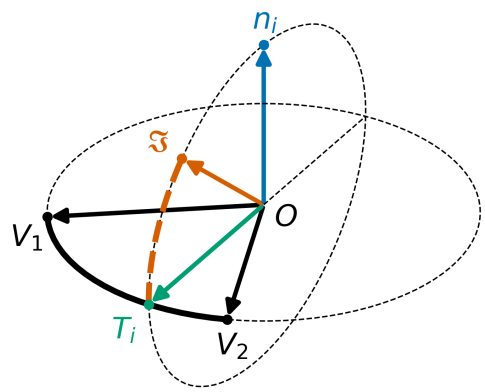

Fig. S2: 3D-representation of the relations between the incenter $\mathfrak{I}$ and a given side $\overline{V_1V_2}$ of the feasibility domain of a 3-species community. The black arrow represents the position of the vertices of the side$\overline{V_1V_2}$, the orange arrow the position of the incenter, the blue arrow the normal vector to the plane that contains the origin (O) and the vertices, and the green arrow the position of the point in the side $\overline{V_1V_2}$ that is tangent to $\mathfrak{I}$, $\mathbf{T}_i$. Finally, the orange dashed arc represents the great circle distance θ between the incerter $\mathfrak{I}$ and side $\overline{V_1V_2}$, that is, the arc $\mathfrak{I}\mathbf{T}_i$.

($S_1 = S_2$) and equal relative volumes ($\Omega_1 = \Omega_2$), since it is closely related to the maximum isotropic perturbation θ that we introduced in the main text.

3 Calculation of the exclusion distance of a given species

Following the notation and arguments introduced in the main text and Suppl. Section 2, the exclusion distance of species i, that is, the great circle distance between an initial vector of intrinsic growth rates $\mathbf{r}_0$ and the border ε_i of the feasibility domain where species i goes excluded, is given by

$$\theta_{0,i} = \sin^{-1}\left(\mathbf{n}_i \cdot \mathbf{r}_0\right), \tag{S7}$$

where $\sin^{-1}(x)$ is the arcsine of x. Note that we simply replaced the incenter $\mathfrak{I}$ in Eqs. (S3) and (S4) by $\mathbf{r}_0$. Then, the position of the tangency point on the edge of the feasibility domain's border ε_i (where species i goes excluded) can be calculated as

$$\mathbf{T}_{0,i} = \mathbf{r}_0 - \sin(\theta_{0,i})\mathbf{n}_i. \tag{S8}$$

To conclude, we relate the point of tangency to the border of the feasibility domain with the minimum exclusion distance described in the main text. If we define the *isotropic feasible domain* of a vector $\mathbf{r}_0$ as the largest set of feasible vectors of intrinsic growth rates that can be achieved by perturbing isotropically (that is, in all directions) the vector $\mathbf{r}_0$, then such domain can be represented as the S-hyperspherical cap that meets the following conditions: i) its apex is $\mathbf{r}_0$, ii) it is tangent to the border of the feasibility domain (at point $\mathbf{r}_{0,\min}$), and iii) has no other points outside the feasibility domain, except those of tangency (see Fig. 2(a) for an example). As pointed out in our theoretical framework (see main text), species exclusion distance θ_0 is the great circle distance between $\mathbf{r}_0$ and the point of tangency $\mathbf{r}_{0,\min}$). That point of tangency to the border of the feasibility domain, $\mathbf{r}_{0,\min}$, is just $\mathbf{r}_{0,\min} = \mathbf{T}_{0,q}$ with $\theta_{0,q} = \min(\theta_{0,i})$ for $i \in \{1, \cdots, S\}$, where $\theta_{0,q} = \theta_0$ defines the size of the minimum perturbation needed to exclude the one species.

4 Estimation of the probabilities of exclusion via simulations of LV dynamics and shape-based calculations

We can compute efficiently the probabilities of exclusion P_i^E by applying the same quasi-Monte Carlo method used to estimate Eq. (4) to both the numerator and denominator in Eq. (8). The results rendered by that approach are in excellent agreement with those obtained from the simulation of the LV model (Eq. 1). The reason is that, given an initial, random vector of intrinsic growth rates ($\mathbf{r}_0$) within the feasibility domain, the trend of species' abundances described by LV dynamics shows that the first species to be excluded matches that of our method, when the species' initial abundances are those of equilibrium ($\mathbf{N}^*$) and $\mathbf{r}_0$ is replaced by the vector of growth rates of the closest point in the border of the feasibility domain ($\mathbf{r}_{0,\min}$) (see panels (b) and (c) in Fig. 2 and Suppl. Fig. S3 for an example).

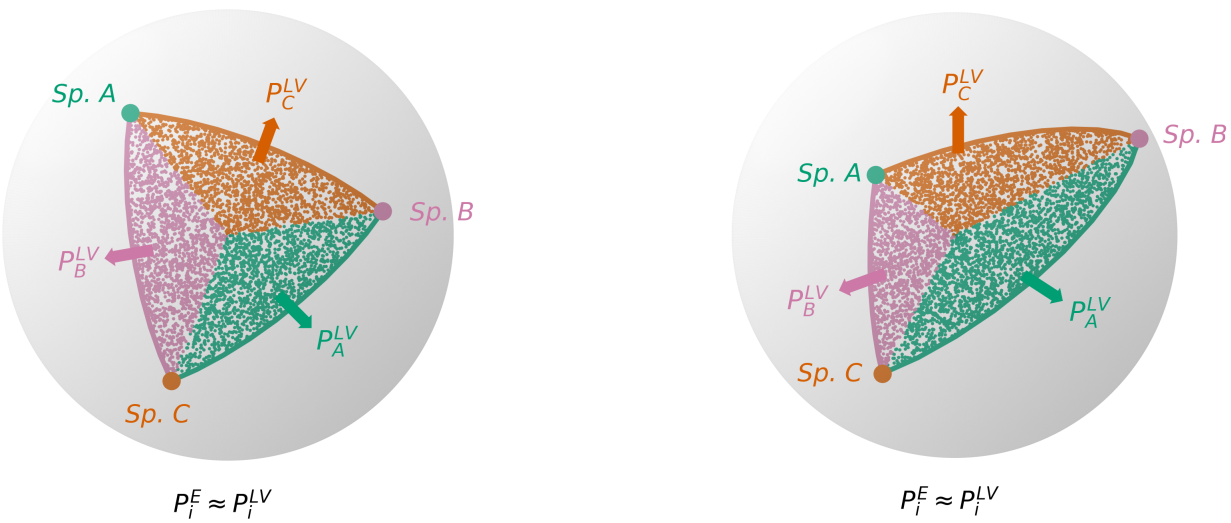

(a) (b)

Fig. S3: (a) Simulation of the first species to be excluded for 5,000 random initial, intrinsic growth rates ($\mathbf{r}_x$) within the feasibility domain shown in Fig. 2(b) by solving the LV equations (see Eq. (1)) when the species' initial abundances are those of equilibrium ($\mathbf{N}^*$) and the initial growth rates $\mathbf{r}_0$ are changed by those of the closest point of tangency in the border of the feasibility domain ($\mathbf{r}_{x,T}$). Colors of points are those of the first species that will be excluded. (e) Same results as in panel (a) for the feasibility domain in Fig. 2(b).

Nevertheless, during the preparation of this work, we have verified that the structure of the

interactions (represented by the interaction matrix $\mathbf{A}$) influences the uncertainty of the above calculations. First, the smaller the size of the feasibility domain (or its relative volume $\Omega(\mathbf{A})$), the more difficult it is to randomly sample. Since the average probabilities of exclusion P_i^E depend on that sampling, the smaller the feasibility domain, the greater the uncertainties of the corresponding sampling, and, hence, the larger those of the probabilities of exclusion of such domains. Second, the more asymmetric the feasibility domain, the more difficult it is to sample the relative volumes of those species with a lower probability of exclusion (i.e., the more difficult it is to sample species that occupy smaller areas in figures analogous to our Fig. 2(c)). Thus, the exclusion probabilities of the potentially more persistent species (those that will have a smaller relative volume within the feasibility domain) will be more uncertain than the exclusion probabilities of the less persistent species (since the latter are easier to randomly sample). Finally, we observed that the differences between LV estimations and those provided by shape-based calculations increase with asymmetry (see Suppl. Fig. S4). However, our tests with symmetric feasibility domains suggest that shape-based calculations are more accurate (see the example for asymmetry index $J'(\mathbf{A}) = 1$ in Suppl. Fig. S4).

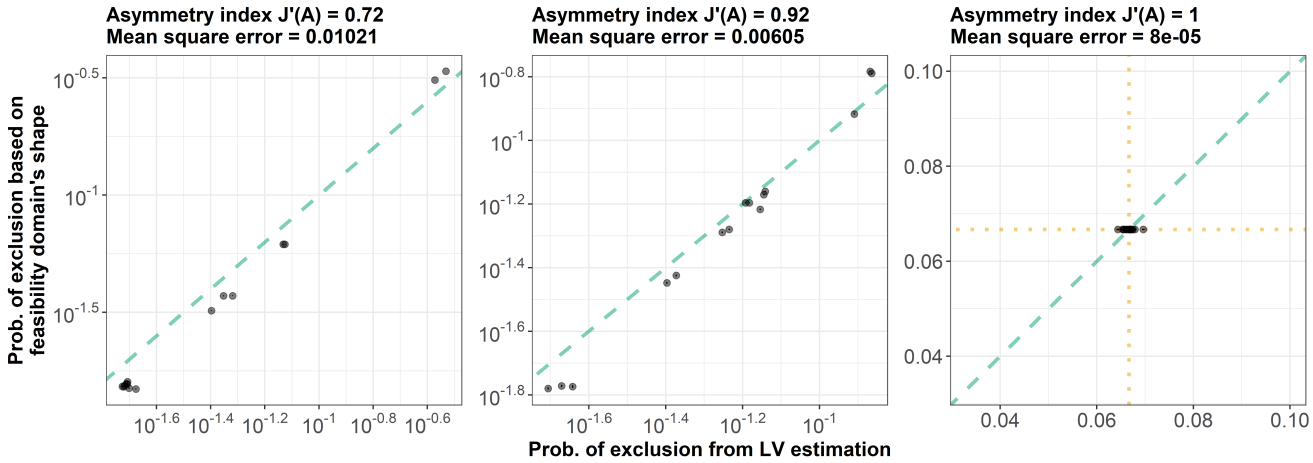

Fig. S4: Comparison between the probabilities of exclusion $P_i^E(\mathbf{A})$ obtained from LV simulations and those estimated with Eqs. (4) and (8). Each panel represents the results a community with $S = 15$ species. The value of the asymmetry index and of the mean square error between the set of probabilities of exclusion are shown in each panel's title. Green dashed line is a guide to the eye that locates probabilities of exclusion that are equal under both calculation approaches, whereas orange dotted line shows the theoretical value of $P_i^E(\mathbf{A})$ for symmetrical feasibility domains, i.e., $P_i^E(\mathbf{A}) = 1/S$ for $J'(\mathbf{A}) = 1$.

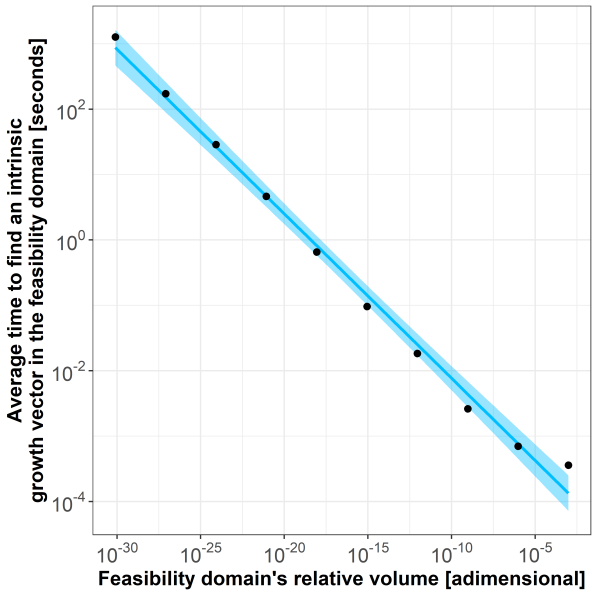

Fig. S5: Dependence of the average computing time (in seconds) for randomly finding feasible intrinsic growth rates in symmetric communities on the feasibility domain's relative volume, $\Omega(\mathbf{A})$ (see Eq. (3)). We used the algorithm "random_feasible_growth_rates" available at `https://github.com/RadicalCommEcol/Asymmetric_Interactions/R/6_computing_times_LV.R`. To test our algorithm we used interaction matrices $\mathbf{A} = -I_S$, where I_S represents a $S \times S$ identity matrix, and S takes the following values: 10, 20, 30, 40, 50, 60, 70, 80, 90 and 100. Blue line shows the fitted regression model computing time $= 10^{-4.62889}\Omega^{-0.25147}$, whereas the blue shade area shows the 95% confidence interval of such model.

5 Testing the dependence of the feasibility asymmetry index on size

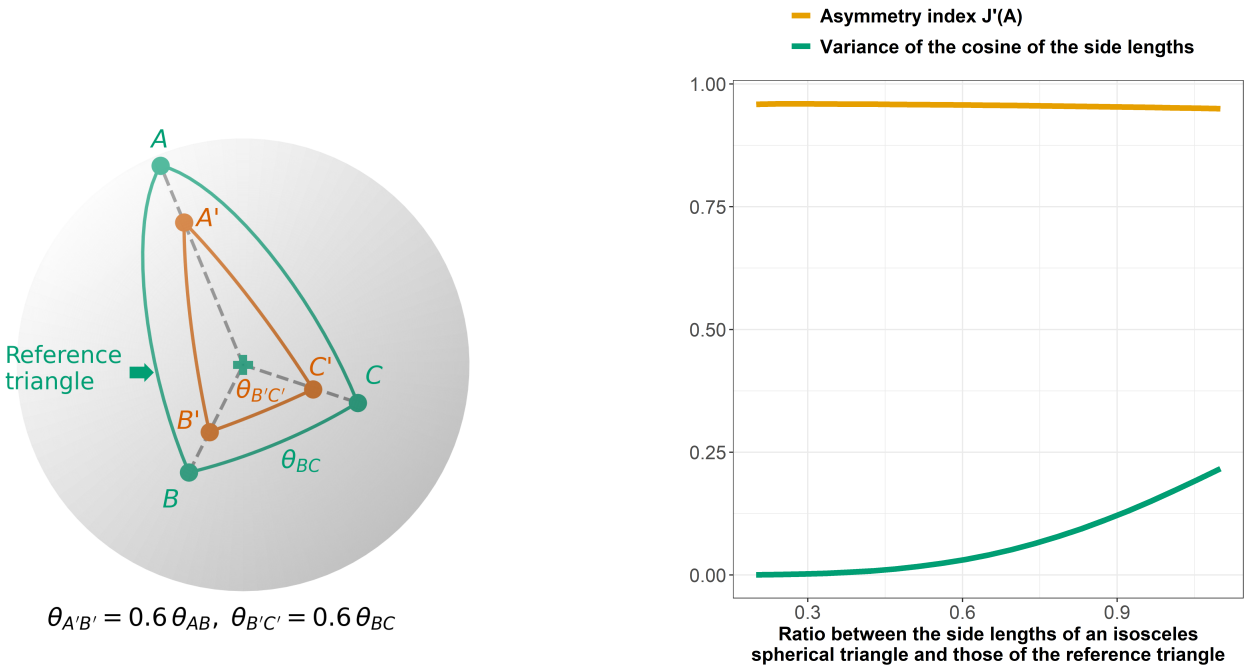

(a) (b)

Fig. S6: (a) An example of (isosceles) spherical triangles with proportional sides. Continuous lines show the border of the respective triangles, dashed lines show the segments of great circles that connect the incenter of the reference triangle (black plus marker) with the vertices of the triangles (orange and green dots, respectively). The ratio between the sides of the orange triangle and those of the green one is equal to 0.6. (b) Comparison of shape indices for isosceles spherical triangles whose side lengths are proportional, like those in Fig. S6(a). The horizontal axis shows the ratio between the side lengths of the spherical triangles tested and those of the reference triangle. Results for the shape index proposed in (Grilli *et al.*, 2017), the variance of the cosine of side lengths, are in green; whereas those for $J'(\mathbf{A})$, obtained with Eq. (9), are in orange.

6 Species information for the empirical example in Caracoles Ranch (Spain)

Table S1: Species studied and their overall abundance (individuals counted) in the whole study area for each year of observations.

Species	Family	2015	2016	2017	2018	2019	2020	2021
Beta macrocarpa	Amaranthaceae	136	1,230	90	20	1,052	2,023	459
Centaurium tenuiflorum	Gentianaceae	1,206	37	1,057	522	705	1,946	1,603
Chamaemelum fuscatum	Asteraceae	5,050	5,802	2,619	0	3,989	1,348	1,451
Chamaemelum mixtum	Asteraceae	882	909	208	2	9	144	68
Hordeum marinum	Poaceae	6,719	13,159	54,264	43,355	71,923	16,780	16,465
Lythrum tribracteatum	Lythraceae	1,321	474	676	3	0	0	0
Leontodon maroccanus	Asteraceae	2,485	3,448	21,657	814	4,182	9,098	11,455
Melilotus elegans	Fabaceae	313	135	2	0	6	1	31
Melilotus sulcatus	Fabaceae	504	414	36	1	1,059	1,106	2,418
Parapholis incurva	Poaceae	1,239	78	2,980	29	7,534	886	678
Plantago coronopus	Plantaginaceae	5,439	518	2,427	1	118	1,134	321
Polypogon maritimus	Poaceae	4,101	709	5,085	315	7,332	3,367	25
Polypogon monspeliensis	Poaceae	442	26	89	1	284	427	78
Pulicaria paludosa	Asteraceae	124	201	2,899	746	739	1418	0
Salsola soda	Amaranthaceae	7,346	490	1,629	4,771	791	2,222	2,821
Scorzonera laciniata	Asteraceae	881	226	85	17	793	1,334	
Sonchus asper	Asteraceae	237	41	0	1	366	1,021	842
Spergularia rubra	Caryophyllaceae	146	103	108	0	550	2,318	102
Suaeda splendens	Amaranthaceae	60	26	0	1	52	99	0

Table S2: Species studied and their average seed survival and germination rates.

Species	Seed survival rate	Germination rate
Beta macrocarpa	0.43	0.38
Centaurium tenuiflorum	0.10	0.53
Chamaemelum fuscatum	0.38	0.08
Chamaemelum mixtum	0.32	0.76
Hordeum marinum	0.25	0.94
Lythrum tribracteatum	0.51	0.62
Leontodon maroccanus	0.33	0.89
Melilotus elegans	0.60	0.59
Melilotus sulcatus	0.63	0.77
Parapholis incurva	0.60	0.33
Plantago coronopus	0.57	0.84
Polypogon maritimus	0.46	0.85
Polypogon monspeliensis	0.49	0.91
Pulicaria paludosa	0.55	0.84
Salsola soda	0.30	0.52
Scorzonera laciniata	0.41	0.69
Sonchus asper	0.29	0.60
Spergularia rubra	0.41	0.44
Suaeda splendens	0.58	0.61

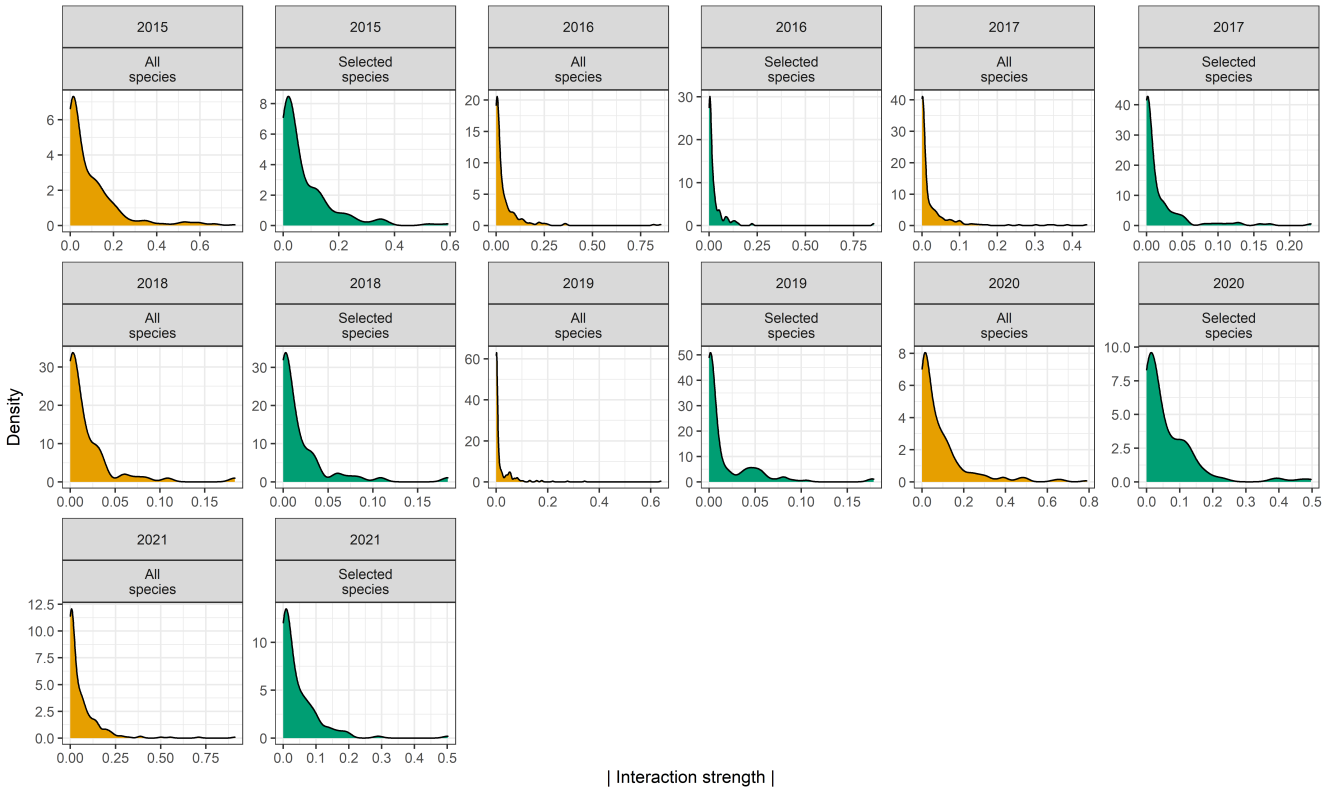

Fig. S7: Distribution of the absolute value of the interaction strengths in Caracoles Ranch across the sampling years. We present the results for the whole set of plant species that were present in a given year (orange fill) and for those seven species that were present all the years (green fill).

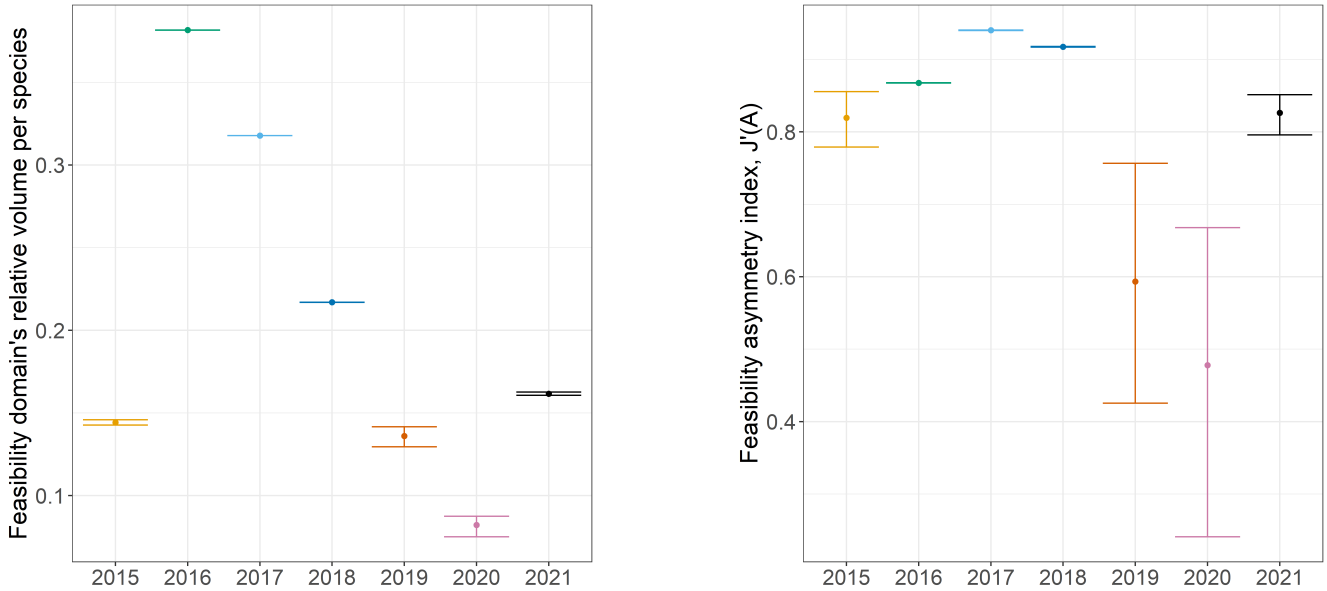

(a) (b)

Fig. S8: (a) Time evolution of the feasibility domain's relative volume per species ($\Omega^{1/S} \in [0, 0.5]$, where S is the total number of species (Song *et al.*, 2018) [see Eqs. (3) and (4)]) for Caracoles Ranch. (b) Feasibility asymmetry index ($J' \in [0, 1]$ [see Eq. (9)]) for the data in panel (a). Error bars in both panels show the 95% confidence intervals for the results of the 10,000 random draws generated to estimate the species' average probability of exclusion ($P_i^E(\mathbf{A})$) each year, by using the quasi-Monte Carlo estimation related to Eq. (4).

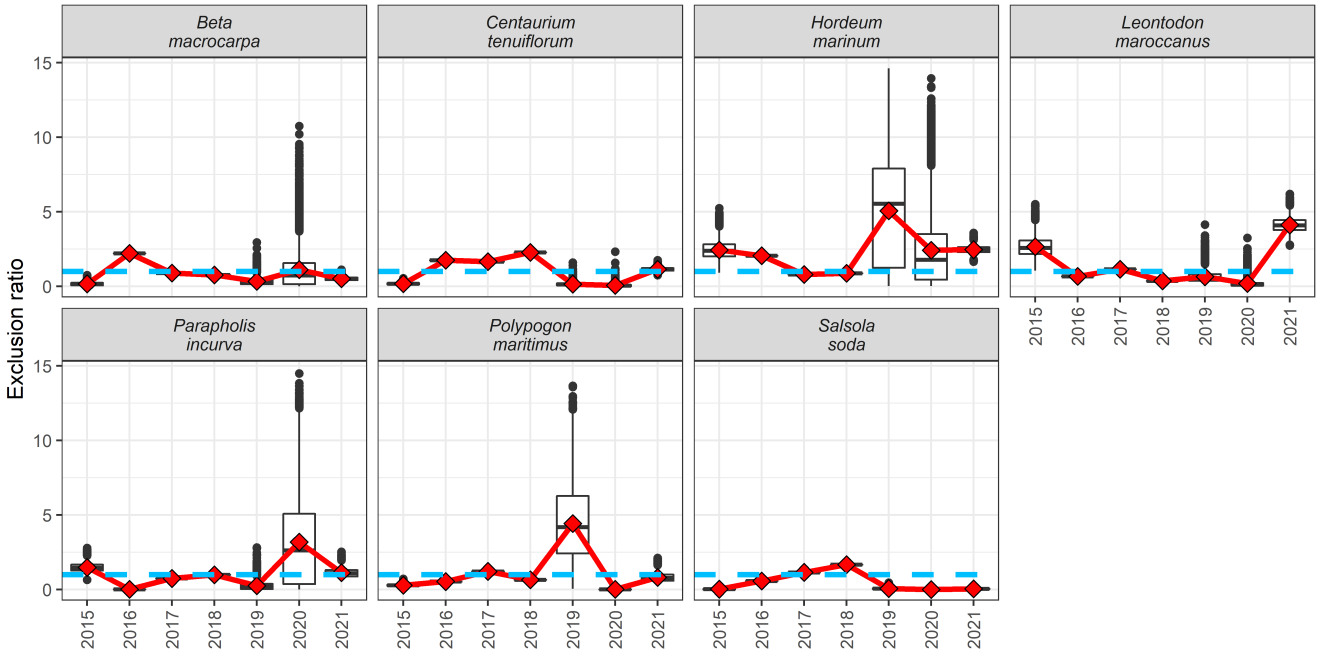

Fig. S9: Time evolution of the exclusion ratio $ER_i(\mathbf{A})$ for each plant species (see Eq. (6)). The box-plots show the results of the 10,000 random draws generated to estimate $P_i^E(\mathbf{A})$ generated each year, by using the quasi-Monte Carlo estimation related to Eq. (4). The red continuous lines connect the mean values of $ER_i(\mathbf{A})$ (red diamonds) from consecutive years, whereas the blue dashed line indicates the region where $ER_i = 1$ (i.e., $P_i^E(\mathbf{A}) = 1/S$). We only show the results for the seven plant species selected for the analyses (see main text).

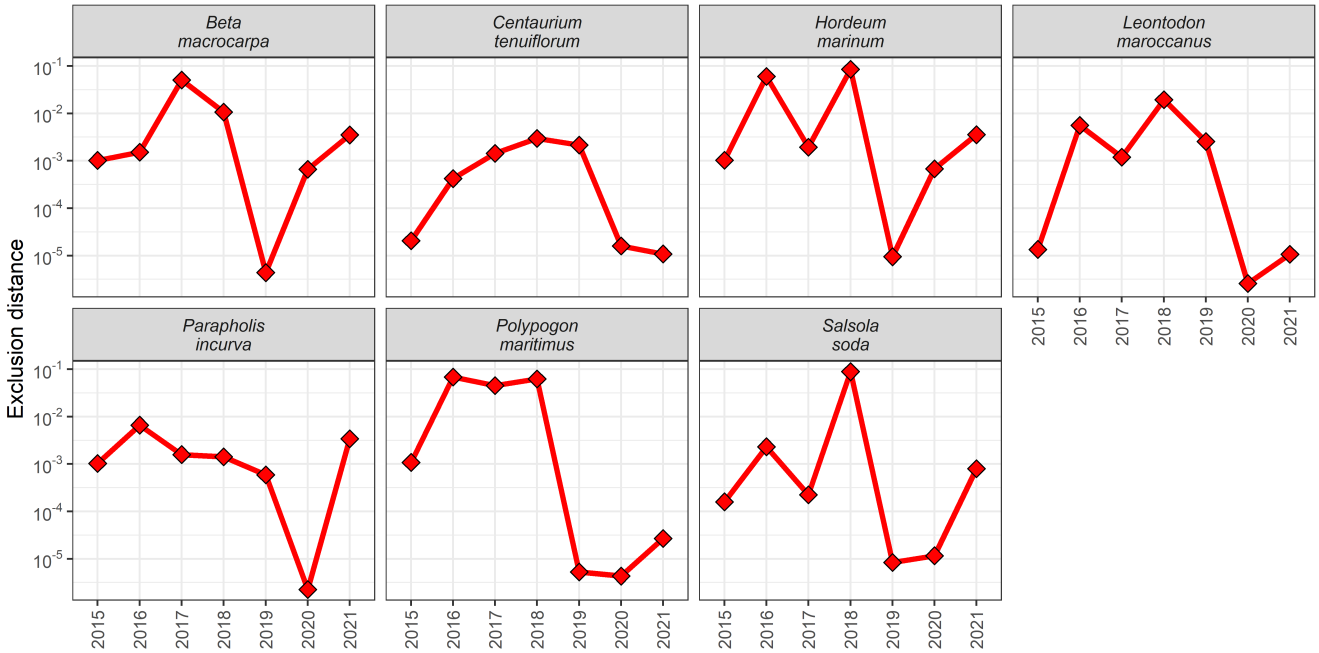

Fig. S10: Time evolution of exclusion distance. The red continuous lines connect the species values (red diamonds) from consecutive years. We only show the results for the seven plant species selected for the analyses (see main text).

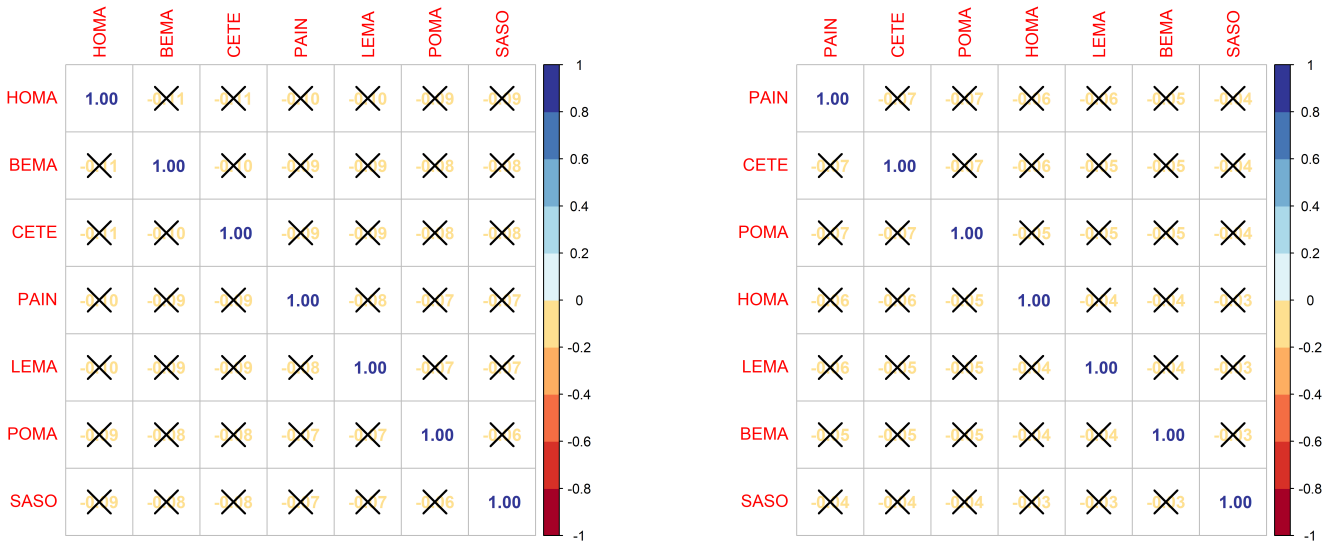

(a) (b)

Fig. S11: a) Correlogram for the time evolution of the mean value of the exclusion ratios shown in Fig. S9. b) Correlogram for the time evolution of the exclusion distances in Fig. S10. Crosses show correlations whose p-value > 0.05.

7 Estimation of the intrinsic growth rates for plant-plant interactions in Caracoles Ranch (Spain)

To estimate the vectors of intrinsic growth rates for the grassland of Caracoles Ranch in a given year, we took advantage of the model formulation for the annual plant considered in (García-Callejas *et al.*, 2021), the Ricker model, and its equivalence to a linear LV model. Following the Suppl. Note 2 in (García-Callejas *et al.*, 2021), it can be easily proved that annual plants have an equivalent intrinsic growth rate, given by:

$$r_i = \lambda_i + \ln\left(\frac{1-(1-g_i)s_i}{g_i}\right). \tag{S9}$$

for species i, where s_i is the survival rate of seeds in the seed bank, g_i is seed germination rate (see)), and λ_i is the number of seeds produced by species i in the absence of interactions. We used the empirical information in table S2 and the file `Data/caracoles_raw_data/lambda_heterogeneous_both.csv` (see our repository) to extract the value of the vector of intrinsic growth rates $\mathbf{r}$ for a given year. Since our framework is developed for feasible equilibrium points, we checked the condition $\mathbf{N}^* = \mathbf{A}^{-1}\mathbf{r} > 0$. If we found a species with negative equilibrium abundance $N_i^* < 0$, we replaced that value by $N_i^{*,mod} = 1$; otherwise, we did nothing (that is, we set $N_i^{*,mod} = N_i^*$). Finally, recalculated the value of $\mathbf{r} = \mathbf{A}\mathbf{N}^{*,mod}$. The code we used can be accessed in our repository at: `R/1c_caracoles_calculate_arc_distances.R`

8 Sampling coverage of Caracoles Ranch (Spain)

We have estimated the sampling coverage of (individual) plant–plant interactions in each year, by pooling the data for all plant species, and using the coverage framework introduced in Chao *et al.* (2014). The sampling coverage (or coverage) of the observed interactions is simply their total relative abundances, or equivalently, the proportion of the total number of interactions in an assemblage that belong to interactions represented in the sample. To calculate the coverage in each plot, we used the R-package `iNEXT` v3.0.0 (Hsieh *et al.*, 2016). As can be seen in Fig. S12, the

sampling coverage from 2015 to 2021 is approximately equal to 99%. This means that less than 1% of the total interactions in the assemblage belong to undetected interactions in a given year. For this reason, extremely rare, undetected interactions do not make a significant contribution to that proportion, even if there are many such interactions. In addition, note that the above estimations do not account for the existence of forbidden interactions, that is, non-occurrences of pairwise interactions that can be accounted for by biological constraints, such as spatio-temporal uncoupling, size or reward mismatching, foraging constraints and physiological–biochemical constraints (Jordano, 2016). Hence, the real sampling coverage of our plant-plant interactions could be higher than 99%.

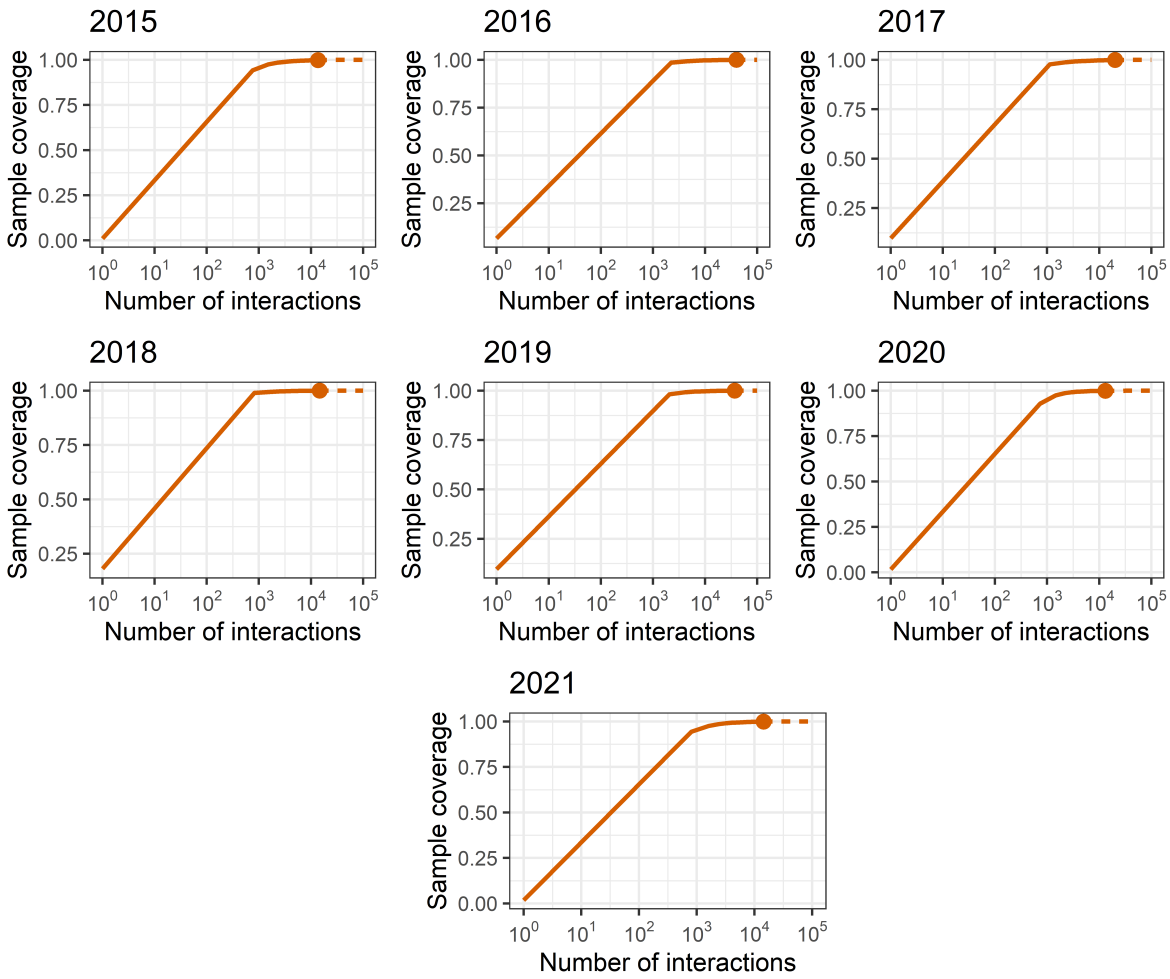

Fig. S12: Sample coverage for rarefied samples (solid line) and extrapolated samples (dashed line) as a function of sample size for plant-plant interactions sampled from each annual community. The 95% confidence intervals were obtained by a bootstrap method based on 1,000 replications. Actual sampling coverage is denoted by solid dots.

9 Results and diagnostics for Caracoles Ranch models

Table S3: Results for the GLM model showing the effect of the plant abundance in a given year on that of next year. We highlighted in bold the most important estimates based on effect sizes and its variability. P-values have been obtained from the Wald test reported in the summary on the models fitted with R-library glmmTMB (Brooks *et al.*, 2017).

Abundance	Estimate	Std. Error	z value	Pr(¿—z—)
(Intercept)	**7.79**	**0.44**	**17.69**	**¡ 2e-16**
Abundance (prev. year)	0.01	0.09	0.16	0.87351
Centaurium tenuiflorum	-0.02	0.57	-0.03	0.97505
Hordeum marinum	**2.47**	**0.50**	**4.94**	**7.8e-07**
Leontodo maroccanus	**1.46**	**0.50**	**2.91**	**0.00362**
Parapholis incurva	0.19	0.56	0.34	0.73486
Polypogon maritimus	0.26	0.56	0.46	0.64427
Salsola soda	0.31	0.56	0.56	0.57416

Table S4: Results for the GLM showing the effect of adding the exclusion ratio in a given year to the model for next year's plant abundance in table S3. We highlighted in bold the most important estimates based on effect sizes and its variability. P-values have been obtained from the Wald test reported in the summary on the models fitted with R-library glmmTMB (Brooks *et al.*, 2017).

Abundance	Estimate	Std. Error	z value	Pr(¿—z—)
(Intercept)	**7.36**	**0.41**	**17.96**	**¡ 2e-16**
Abundance (prev. year)	**0.21**	**0.08**	**2.56**	**0.010580**
Excl. ratio (prev. year)	**-0.56**	**0.13**	**-4.29**	**1.72e-05**
Centaurium tenuiflorum	-0.17	0.55	-0.30	0.762262
Hordeum marinum	**3.13**	**0.45**	**6.97**	**3.14e-12**
Leontodon maroccanus	**1.69**	**0.45**	**3.78**	**0.000158**
Parapholis incurva	0.33	0.52	0.62	0.532456
Polypogon maritimus	-0.01	0.54	-0.01	0.987782
Salsola soda	-0.17	0.52	0.32	0.747773

Table S5: Results for the GLM showing the effect of adding the exclusion distance in a given year to the model for next year's plant abundance in table S3. We highlighted in bold the most important estimates based on effect sizes and its variability. P-values have been obtained from the Wald test reported in the summary on the models fitted with R-library glmmTMB (Brooks *et al.*, 2017).

Abundance	Estimate	Std. Error	z value	Pr(¿—z—)
(Intercept)	**7.47**	**0.40**	**18.63**	**¡ 2e-16**
Abundance (prev. year)	0.01	0.07	0.07	0.940500
Excl. distance (prev. year)	**0.42**	**0.07**	**5.93**	**2.95e-09**
Centaurium tenuiflorum	0.01	0.53	0.01	0.989938
Hordeum marinum	**2.53**	**0.45**	**5.65**	**1.56e-08**
Leontodon maroccanus	**1.71**	**0.44**	**3.86**	**0.000115**
Parapholis incurva	0.27	0.52	0.52	0.602659
Polypogon maritimus	0.19	0.50	0.39	0.697325
Salsola soda	-0.28	0.55	-0.52	0.606811

Table S6: AIC comparison among the candidate for the plant abundance in Caracoles Ranch (see main text). In this table, AIC_i is the AIC of the i-th model, AIC_{min} is the lowest AIC one obtains among the set of models examined, and Δ_i is given by $\Delta_i = AIC_i - AIC_{min}$.

Model	Degrees of freedom	AIC_i	Δ_i
Abundance	9	665.85	19.11
Abundance + Excl. ratio	10	654.63	7.90
Abundance + Excl. distance	10	646.74	0

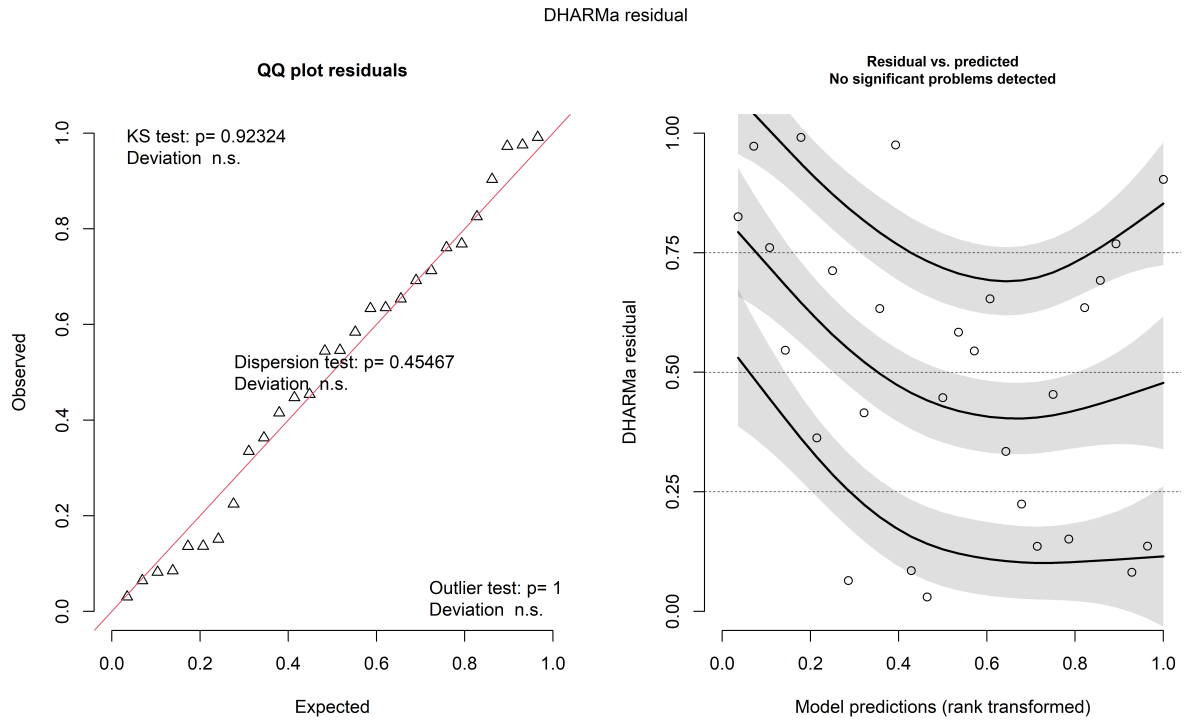

Fig. S13: Diagnostic results obtained from "DHARMa" (Hartig, 2022) for the model that includes the exclusion ratio among its independent variables. Left panel shows the qq-plot for scaled residuals to detect overall deviations from the expected distribution, by default with added tests for correct distribution (KS test), dispersion and outliers. As can be seen, tests don't detect significant deviations from the desired behavior. Right panel reproduces a plot of the residuals against the predicted value. No significant problems nor simulation outliers have been detected.

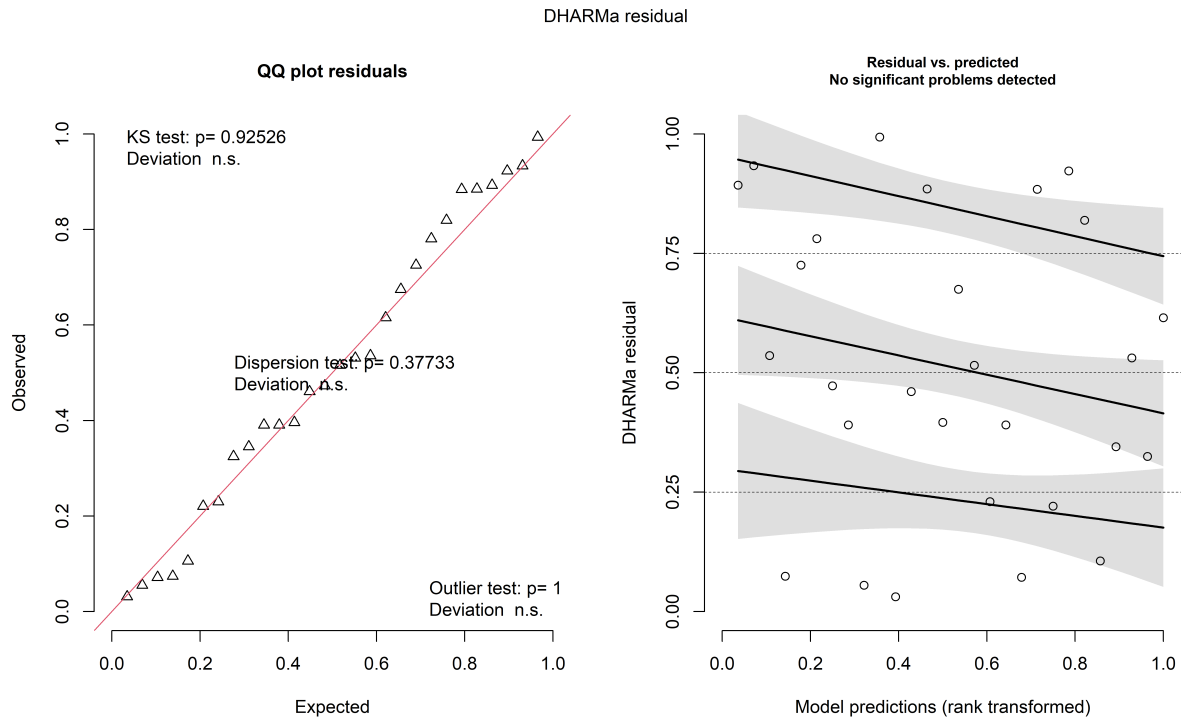

Fig. S14: Diagnostic results obtained from "DHARMa" (Hartig, 2022) for the model that includes the exclusion distance among its independent variables. Tests and results are similar to those in Fig. S13.

10 Results for bipartite plant-pollinator networks in Mangal

Table S7: List of studies in Mangal database (Poisot *et al.*, 2016) ordered by author with the year of publication, number of contributed networks and digital object identifier (DOI).

First author	Number of networks	Year	DOI
Bartomeus	12	2008	10.1007/s00442-007-0946-1
Bezerra	1	2009	10.1111/j.1365-2656.2009.01567.x
CaraDonna	25	2020	10.1111/ele.12740
Kaiser-Bunbury	1	2014	10.1890/14-0024.1
Ponisio	49	2017	10.1111/ele.12821

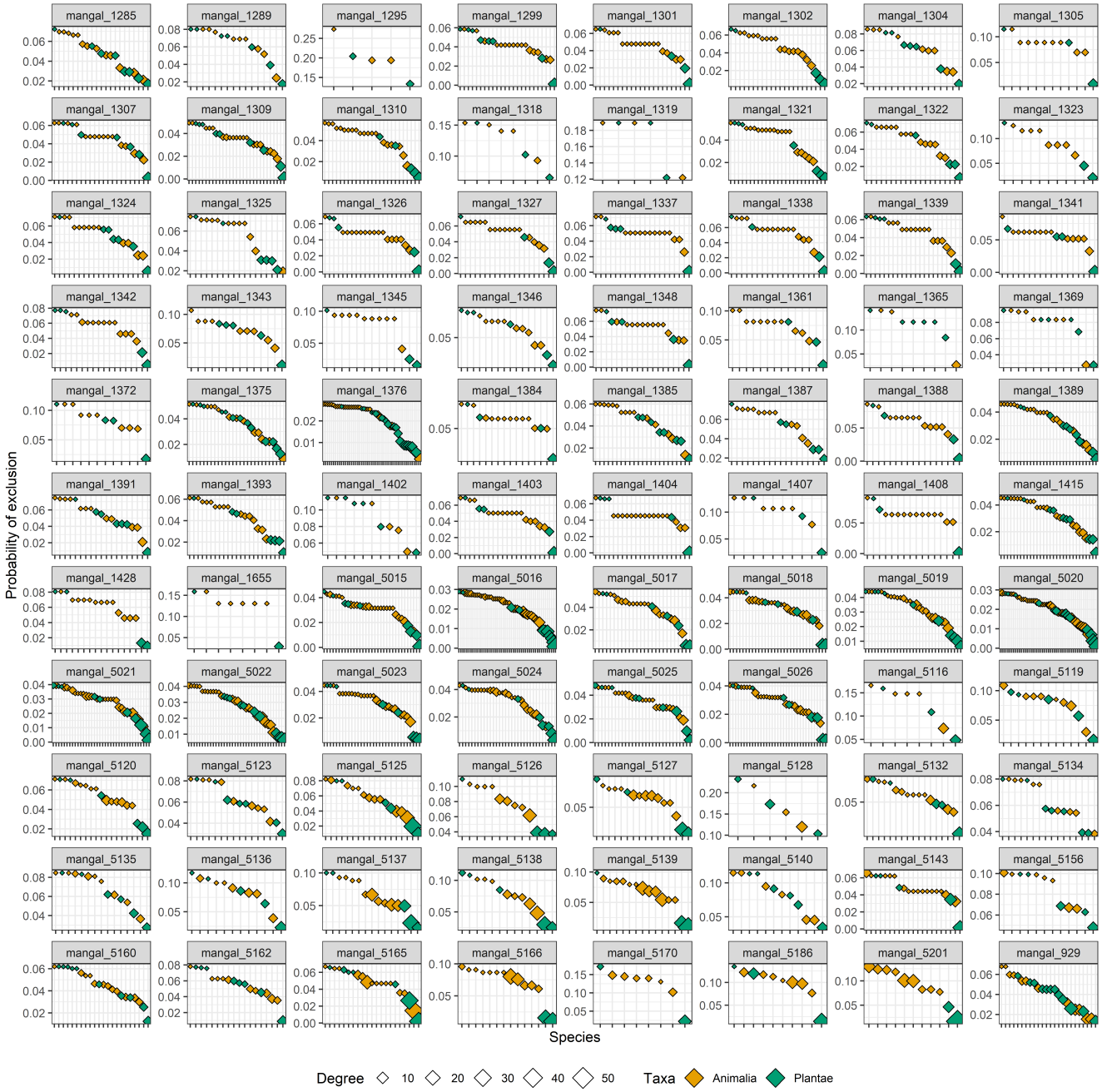

Fig. S15: Average probability of exclusion, $P_i^E(\mathbf{A})$ [Eq. (8)], for a sample of 88 bipartite networks, extracted from Mangal (Poisot *et al.*, 2016). To create the corresponding interaction matrices, we used the mean-field approach in (Saavedra *et al.*, 2016) for systems with no interspecific competition, namely: $\rho = 0.00$, $\delta = 0.25$ and $\gamma_0 = 0.50\,\langle\gamma_{ij}\rangle$ (see further details on the parameters in the referred paper). In each network (panel), the color and the size of markers show node's taxa and degree, respectively.

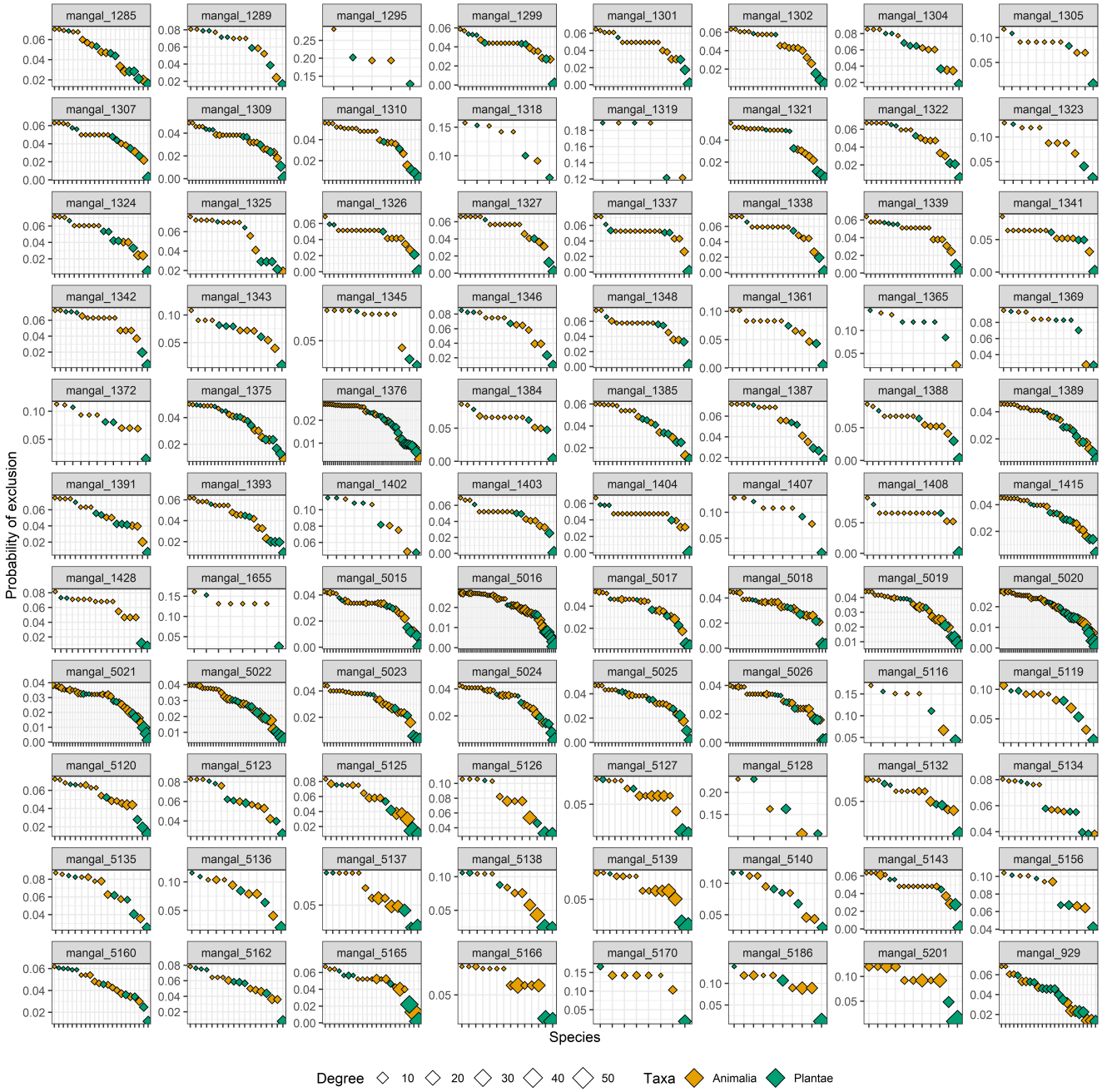

Fig. S16: Average probability of exclusion, $P_i^E(\mathbf{A})$ [Eq. (8)], for a sample of 88 bipartite networks, extracted from Mangal (Poisot *et al.*, 2016). To create the corresponding interaction matrices, we used the mean-field approach in (Saavedra *et al.*, 2016) for systems with no mutualistic trade-off, namely: $\rho = 0.01$, $\delta = 0.00$ and $\gamma_0 = 0.50\,\langle\gamma_{ij}\rangle$ (see further details on the parameters in the referred paper). In each network (panel), the color and the size of markers show node's taxa and degree, respectively.

Supplementary References

Brooks, M. E., Kristensen, K., van Benthem, K. J., Magnusson, A., Berg, C. W., Nielsen, A., Skaug, H. J., Maechler, M. & Bolker, B. M. (2017). glmmTMB balances speed and flexibility among packages for zero-inflated generalized linear mixed modeling. *The R Journal*, 9, 378–400.

Chao, A., Gotelli, N. J., Hsieh, T. C., Sander, E. L., Ma, K. H., Colwell, R. K. & Ellison, A. M. (2014). Rarefaction and extrapolation with hill numbers: A framework for sampling and estimation in species diversity studies. *Ecological Monographs*, 84, 45–67.

García-Callejas, D., Bartomeus, I. & Godoy, O. (2021). The spatial configuration of biotic interactions shapes coexistence-area relationships in an annual plant community. *Nature Communications*, 12.

Grilli, J., Adorisio, M., Suweis, S., Barabás, G., Banavar, J. R., Allesina, S. & Maritan, A. (2017). Feasibility and coexistence of large ecological communities. *Nature Communications*, 8.

Hartig, F. (2022). *DHARMa: Residual Diagnostics for Hierarchical (Multi-Level / Mixed) Regression Models*. URL `https://CRAN.R-project.org/package=DHARMa`. R package version 0.4.5.

Hsieh, T. C., Ma, K. H. & Chao, A. (2016). inext: An r package for rarefaction and extrapolation of species diversity (hill numbers). *Methods in Ecology and Evolution*, 7, 1451–1456.

Jordano, P. (2016). Sampling networks of ecological interactions. *Functional Ecology*, 30, 1883–1893.

Li, S. (2010). Concise formulas for the area and volume of a hyperspherical cap. *Asian Journal of Mathematics and Statistics*, 4, 66–70.

Poisot, T., Baiser, B., Dunne, J. A., Kéfi, S., Massol, F., Mouquet, N., Romanuk, T. N., Stouffer, D. B., Wood, S. A. & Gravel, D. (2016). Mangal – making ecological network analysis simple. *Ecography*, 39, 384–390.

Saavedra, S., Rohr, R. P., Olesen, J. M. & Bascompte, J. (2016). Nested species interactions promote feasibility over stability during the assembly of a pollinator community. *Ecology and Evolution*, 6, 997–1007.

Song, C., Rohr, R. P. & Saavedra, S. (2018). A guideline to study the feasibility domain of multi-trophic and changing ecological communities. *Journal of Theoretical Biology*, 450, 30–36.